© 2021. Published by The Company of Biologists Ltd | Development (2021) 148, dev193227. doi:10.1242/dev.193227

RESEARCH ARTICLE

Retinoic acid production, regulation and containment through Zic1, Pitx2c and Cyp26c1 control cranial placode specification

Aditi Dubey[1], Jianshi Yu[2], Tian Liu[2], Maureen A. Kane[2] and Jean-Pierre Saint-Jeannet[1,*]

ABSTRACT

All paired sensory organs arise from a common precursor domain called the pre-placodal region (PPR). In *Xenopus*, Zic1 non-cell autonomously regulates PPR formation by activating retinoic acid (RA) production. Here, we have identified two Zic1 targets, the RA catabolizing enzyme Cyp26c1 and the transcription factor Pitx2c, expressed in the vicinity of the PPR as being crucially required for maintaining low RA levels in a spatially restricted, PPR-adjacent domain. Morpholino- or CRISPR/Cas9-mediated Cyp26c1 knockdown abrogated PPR gene expression, yielding defective cranial placodes. Direct measurement of RA levels revealed that this is mediated by a mechanism involving excess RA accumulation. Furthermore, we show that *pitx2c* is activated by RA and required for Cyp26c1 expression in a domain-specific manner through induction of FGF8. We propose that Zic1 anteriorly establishes a program of RA containment and regulation through activation of Cyp26c1 and Pitx2c that cooperates to promote PPR specification in a spatially restricted domain.

KEY WORDS: Retinoic acid, Placode, *Xenopus*, Degradation, Patterning

INTRODUCTION

Paired sensory organs in vertebrates originate from thickenings of the embryonic head ectoderm called cranial placodes (Le Douarin, 1986; Saint-Jeannet and Moody, 2014). All cranial placodes arise from a common progenitor territory known as the pre-placodal region (PPR). In *Xenopus*, the PPR is located adjacent to the anterior neural plate (ANP) (Schlosser and Ahrens, 2004). A combination of inductive signaling events and transcriptional programs result in the progressive subdivision of the PPR into distinct placodal regions that subsequently adopt fates characteristic of adenohypohyseal, olfactory, lens, trigeminal, epibranchial and otic placodes along the antero-posterior axis (Schlosser, 2006; Baker and Bronner-Fraser, 2001; Grocott et al., 2012). Given these diverse contributions, disruptions in the specification of the PPR can lead to an array of congenital disorders in humans affecting the orofacial complex, such as blindness, deafness, anosmia, hormone imbalances and sensory deficits (Xu et al., 2002; Ruf et al., 2004; Schönberger et al., 2005; Li et al., 2010; Moody and LaMantia, 2015). Understanding the development of placodes is therefore crucially important to decipher the underlying causes of these disorders.

[1]Department of Molecular Pathobiology, New York University College of Dentistry, New York, NY 10010, USA. [2]Department of Pharmaceutical Sciences, University of Maryland School of Pharmacy, Baltimore, MD 21201, USA.

*Author for correspondence (jsj4@nyu.edu)

A.D., 0000-0002-1030-1347; M.A.K., 0000-0002-5525-9170; J.-P.S., 0000-0003-3259-2103

Handling Editor: Patrick Tam
Received 22 May 2020; Accepted 12 January 2021

Retinoic acid (RA) is a well-documented morphogen during vertebrate development (Duester, 2008), and is especially crucial for the formation of head structures (Dubey et al., 2018). In the context of cranial placodes, RA signaling through RA receptor α2 (RARα2) has been implicated in the establishment of the posterior-lateral boundary of the PPR in *Xenopus* (Janesick et al., 2012). Later in development, RA signaling regulates the formation of several placode derivatives. For example in the chick, otic placode morphogenesis and patterning depends on adjacent domains of RA synthesis and degradation that are crucial to establishing the anterior and posterior domains of the inner ear (Bok et al., 2011). In both chick and mouse, the olfactory epithelium is an important source of RA, and in the absence of RA olfactory progenitors fail to expand and to differentiate into olfactory neurons (Paschaki et al., 2013).

Previous work from our laboratory has demonstrated that the transcription factor Zic1 is necessary and sufficient to specify placode fate through activation of PPR-specific genes such as *Six1* and *Eya1* (Hong and Saint-Jeannet, 2007). Interestingly, Zic1 is not expressed in the PPR and a microarray screen to identify its downstream targets uncovered a novel, non-cell autonomous role for Zic1 in the specification of PPR (Bae et al., 2014; Jaurena et al., 2015). Specifically, Zic1 at the ANP is required for the activation of the retinoic acid (RA)-synthesizing enzyme, retinaldehyde dehydrogenase 2 (ALDH1A2) and the RA transporter, lipocalin-prostaglandin D2 synthase (LPGDS), effectively creating an anterior source of RA in the embryo (Jaurena et al., 2015). Disruptions in the function of these two factors diminished the expression of PPR genes, indicating a crucial role for RA in PPR formation. This work showed that not only is RA signaling required for PPR formation, but also that PPR gene activation depends on specific levels of RA. Given the acute sensitivity of the PPR to RA levels, this suggested that a careful calibration and containment of RA signaling likely takes place to allow for the appropriate specification of the PPR. This prompted us to investigate the existence of a possible RA-regulation program between the PPR and the ANP, where RA levels are locally established and maintained.

Here, we have analyzed the function of another Zic1 target, the RA-catabolizing enzyme Cyp26c1, which is expressed anteriorly in the vicinity of the PPR. We show that Cyp26c1 is not only crucial for PPR and cranial placode development, but also broadly for the formation of anterior structures. Direct measurement of RA levels by LC-MS/MS revealed that RA levels are abnormally elevated in *cyp26c1*-depleted embryos. Additionally, we show that, rather than an absence of RA, this region needs to maintain low RA levels compatible with PPR gene expression. Furthermore, we show that Cyp26c1 expression anteriorly is regulated by the transcription factor Pitx2c, an RA-responsive gene and a Zic1 target, through the activation of FGF signaling. Thus, these events set in motion by Zic1 induction serve to create a robust anterior RA gradient that is essential for placode specification. Collectively, our results uncover a novel program of RA containment and regulation through Cyp26c1 and Pitx2c that cooperates to promote PPR specification in a spatially restricted domain.

Development (2021) 148, dev193227. doi:10.1242/dev.193227

RESULTS

Cyp26c1 is expressed anteriorly and is a target of Zic1

We have previously identified the RA catabolizing enzyme Cyp26c1 as a target of Zic1 during PPR formation in a microarray screen (Bae et al., 2014; Jaurena et al., 2015). At the neurula stage, *cyp26c1* is expressed in the prospective hindbrain and anteriorly in a region that abuts the neural plate, consistent with a potential role in PPR formation (Fig. 1A; Tanibe et al., 2008). In order to confirm that Cyp26c1 is a genuine target of Zic1, we analyzed its regulation by Zic1 in the embryo. Zic1 overexpression (Zic1GR; Hong and Saint-Jeannet, 2007) resulted in expansion of *cyp26c1* expression domains (Fig. 1B,C). Conversely, Zic1 knockdown (Zic1MO; Sato et al., 2005) showed reduction in *cyp26c1* expression domains (Fig. 1B,C). Furthermore, in animal cap explants, Zic1GR expression is sufficient to activate *cyp26c1*, whereas it has no impact on the related enzyme, *cyp26a1* (Fig. 1D,E). These observations indicate that Zic1 is necessary and sufficient for *cyp26c1* expression.

To understand the developmental dynamics of *cyp26c1* expression, we used qRT-PCR to compare its temporal expression to that of *six1*, a PPR gene, and of *pitx2c* (Jeong et al., 2014), a transcription factor that is a putative Zic1 target (Bae et al., 2014; Jaurena et al., 2015). *cyp26c1* is activated shortly after mid-blastula transition and progressively increases until stage 22, followed by a decrease in expression over time (Fig. 1F; Fig. S1), whereas *six1* and *pitx2c* show a steadier increase throughout development (Fig. 1G,H; Fig. S1).

Consistent with previous reports (Tanibe et al., 2008; Yu et al., 2016), *cyp26c1* is first detected by *in situ* hybridization (ISH) at the gastrula stage (Fig. 1I; stage 12) in a single domain that, as development proceeds, segregates into two regions: the prospective hindbrain posteriorly and in a crescent-shaped domain anteriorly (Fig. 1I). We compared the expression of *cyp26c1* with that of *pitx2c*, which is expressed in a similar region of the ectoderm (Jeong et al., 2014). We found that *pitx2c* expression is confined to this crescent-shaped domain and temporally precedes *cyp26c1* in this region that later maps to the prospective cement gland (Fig. 1I).

Two-color *in situ* hybridization reveals that the *cyp26c1* anterior expression domain abuts, but does not overlap with, the *zic1* expression domain, whereas both genes are co-expressed in the

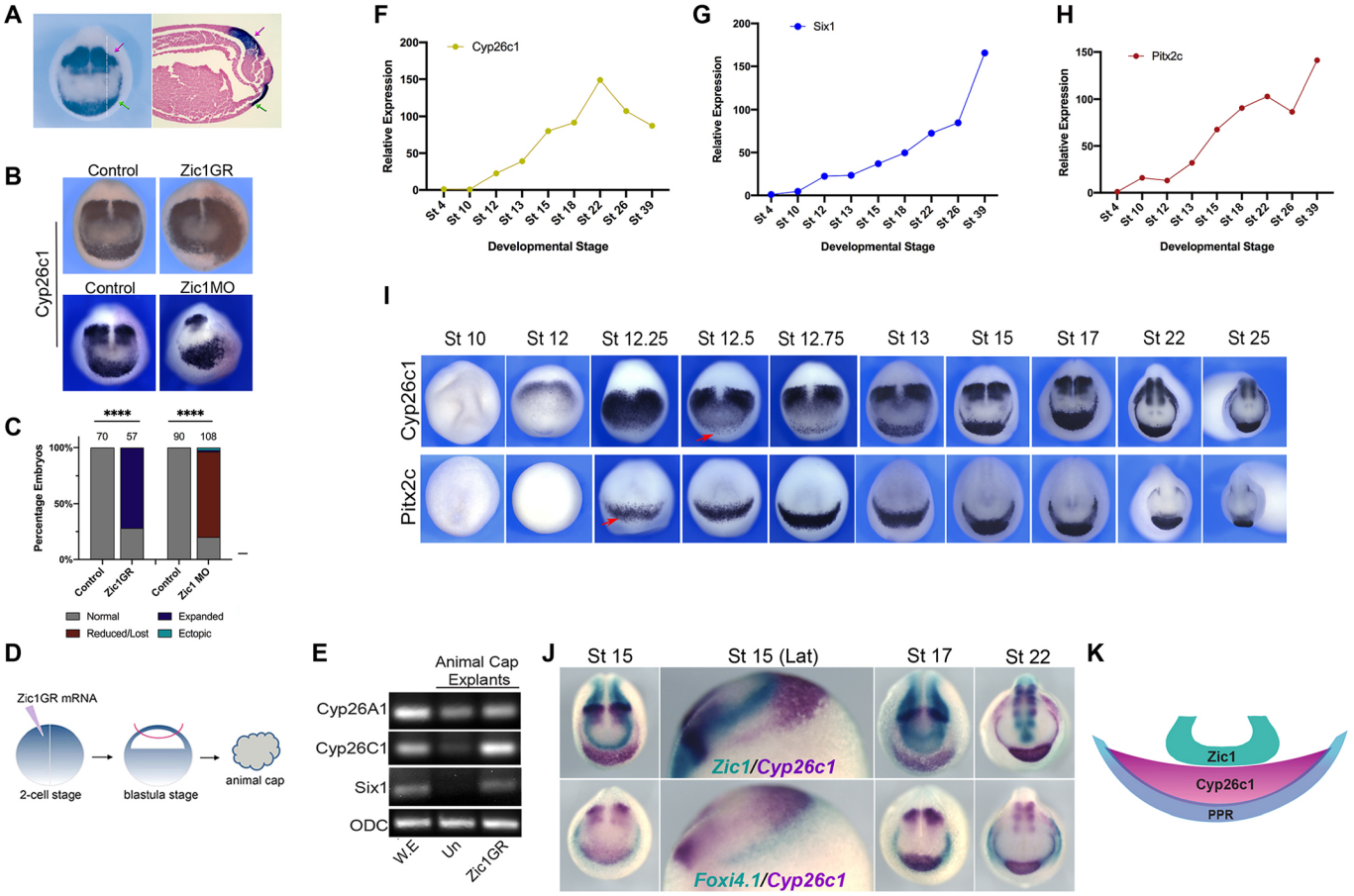

Fig. 1. Cyp26c1 is expressed anteriorly and is a target of Zic1. (A) *In situ* hybridization for *cyp26c1* expression at late neurula stage (left panel). The dashed white line indicates the plane of section. Right panel shows the corresponding section (lateral view) stained with Hematoxylin and Eosin. The prospective hindbrain (magenta arrow) and the PPR-adjacent anterior (green arrow) domains are indicated. (B) *In situ* hybridization for *cyp26c1* on control, Zic1GR- and Zic1MO-injected embryos (upper panel). Representative images are shown, with the injected side on the right. (C) Quantification of the phenotypes. The number of embryos analyzed for each condition is on the top of each bar; ****P<0.0001, χ^2 test. (D) Schematic representation of an animal cap explant assay. (E) RT-PCR analysis of *cyp26c1*, *cyp26a1*, *six1* and *ODC* (ornithine decarboxylase 1) expression in Zic1GR-injected animal cap explants. (F,G,H) Developmental qRT-PCR expression profile of *cyp26c1* (F), *six1* (G) and *pitx2c* (H). NF stages are indicated on the *x*-axis, values are normalized to ODC. A representative experiment is shown. (I) *In situ* hybridization for *cyp26c1* and *pitx2c* expression. NF stages are indicated at the top of each panel. The onset of expression of *cyp26c1* and *pitx2c* in the PPR-adjacent domain is indicated with a red arrow. (J) Double *in situ* hybridization for *zic1* (teal) and *cyp26c1* (magenta) (upper panels); and *foxi4.1* (teal) and *cyp26c1* (magenta) (lower panels). Higher magnifications of stage 15 embryos are shown. (K) Schematic representation of *zic1*, *cyp26c1* and *foxi4.1* expression domains. (E) W.E, whole embryo; (J) Lat, lateral view. All images show anterior views with dorsal towards the top, unless otherwise indicated.

Development (2021) 148, dev193227. doi:10.1242/dev.193227

prospective hindbrain region (Fig. 1J; upper panels). When compared with the PPR gene *foxi4.1*, the *cyp26c1* expression domain appears to line and partially overlap with the *foxi4.1* posterior expression domain (Fig. 1J; lower panels). Therefore, anteriorly *cyp26c1* is nested in a region between the *zic1* and *foxi4.1* expression domains (Fig. 1K).

To further establish that Cyp26c1 expression at these development stages is directly relevant to RA metabolism, we used LC-MS/MS for whole-embryo measurements of endogenous levels of all-trans RA (at-RA) and 4-oxo-RA, a major RA metabolite generated by Cyp26 enzymes (Pijnappel et al., 1993; Baron et al., 2005) (Fig. 2A). We found that whereas at-RA is detected at similar levels at NF stages 9 and 10.5, when *cyp26c1* is undetectable (Fig. 1F,I), at NF stage 13, when *cyp26c1* is robustly expressed, at-RA levels showed a marked decrease (Fig. 2B). This reduction in at-RA is accompanied by a significant increase in 4-oxo-RA at this stage (Fig. 2C). We also quantified 13-cis-RA, a RA isomer with low affinity for nuclear receptors, and the RA precursors retinol and retinyl ester (RE), which were statistically unchanged across stages 9, 10.5 and 13 (Fig. S2). Collectively, these findings indicate that, at NF stage 13, Cyp26c1 participates in the regulation of at-RA levels in the whole embryo.

Cyp26c1 knockdown results in a broad loss of anterior structures

Based on the spatial expression profile of *zic1*, *cyp26c1* and *foxi4.1*, we have updated our model of PPR specification by RA (Jaurena et al., 2015) (Fig. 3A), and propose that Cyp26c1 may serve to establish an RA refractory region between the RA-synthesizing ANP, and the RA-responsive PPR in order to properly position this domain. This model predicts that there are two pools of RA produced at the anterior neural plate: a pool bound to lipocalin-type prostaglandin D2 synthase (LPGDS), which is resistant to Cyp26c1 activity and that can travel to the prospective PPR region to activate placode genes; and an unbound pool that is actively degraded by Cyp26c1 in order to maintain low levels required for PPR specification (Fig. 3A).

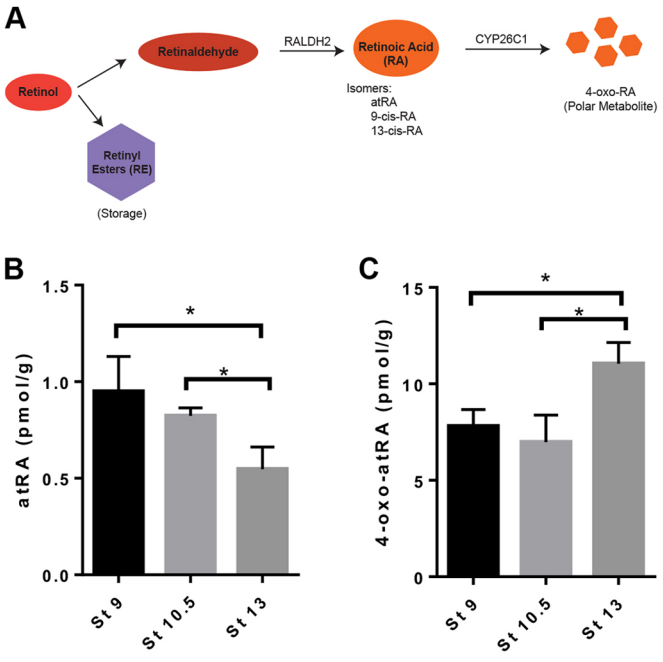

Fig. 2. Measurement of at-RA and 4-oxo RA levels in the embryo. (A) Schematic representation of the metabolic pathway for synthesis and degradation of endogenous RA by RALDH2 and Cyp26c1, respectively. (B,C) Endogenous retinoids, at-RA (B) and 4-oxo-RA (C), in wild-type *Xenopus* embryo at stages 9, 10.5 and 13, as quantified by LC-MS/MS. NF stages are indicated on the *x*-axis. Data are for 130 embryos per group and are shown as mean±s.d., n=3 groups per time-point; *P<0.0311 (unpaired t-test).

To evaluate the role of Cyp26c1 in PPR specification, we used a morpholino (MO) antisense oligonucleotide targeting the intron 4/exon 5 junction of *cyp26c1* pre-mRNA (Cyp26MO; Fig. 3B) to interfere with its function. Injection of increasing amounts of Cyp26c1MO in the embryo resulted in the accumulation of an aberrant transcript due to intron 4 retention (Fig. 3B). Based on sequence analysis, the retention of this intron is predicted to generate a truncated Cyp26c1 protein lacking the C-terminal domain that is responsible for the enzymatic activity of Cyp26c1; however, this could not be confirmed by western blot due to the lack of suitable antibody to detect endogenous Cyp26c1 in *Xenopus*. Unilateral injection of Cyp26MO resulted in a significant reduction of *six1*, *foxi4.1* and *dmrta1* expression at the PPR, as well as a reduction of the placodal expression domain of *sox2* (Fig. 3C-E). These findings were further confirmed in animal cap explants, where the induction of *six1* and *pitx2c* by Zic1GR was strongly inhibited in the presence of Cyp26c1MO (Fig. 3F,G; Fig. S3).

In order to assess the long-term consequences of Cyp26c1 depletion on cranial placode formation, embryos bilaterally injected with Cyp26MO at the two-cell stage were analyzed at early to late tailbud stages (NF stage 26-31; Fig. 3H,I). Strikingly, *six1* expression was severely reduced in all placodal domains, including the epibranchial and olfactory placodes (Fig. 3H,I) (Schlosser and Ahrens, 2004). The expression of *foxi4.1* in epibranchial placodes was also reduced and their spatial organization was severely disrupted (Fig. 3H,I). These embryos also had defective lens and otic placodes, as visualized by the expression of *tbx2* (Fig. 3H,I; Takabatake et al., 2000).

We also performed Cyp26c1 knockdown using the CRISPR-Cas9 gene-editing technology. The Cyp26c1 mutations in the CRISPR-Cas9-injected embryos were confirmed by direct sequencing of PCR products (DSP) assay (Fig. S4). Unilateral co-injections of two single guide RNAs (sgRNAs) targeting exon 1 and exon 2 with Cas9 protein resulted in a marked reduction of *six1* and *foxi4.1* expression when compared with Cas9-only injected siblings (Fig. 3J,K). Approximately 25% of the embryos show an expansion of *foxi4.1*. Because each mutation event is unique in cyp26c1-CRISPR embryos (Fig. S4), and likely to differently affect cyp26c1 function, we can speculate that, in some embryos, *cyp26c1* mutations may lead to a partial attenuation of Cyp26c1 activity, resulting in accumulation of RA to levels compatible with *foxi4.1* expansion, as observed in embryos exposed to low doses of RA (Jaurena et al., 2015). Therefore, using two different approaches to interfere with Cyp26c1 function, we were able to establish the requirement of Cyp26c1 activity for PPR gene expression and the development of anterior structures, including multiple cranial placodes.

Although animal cap explants expressing Zic1 are fated to generate placode progenitors in the absence of other tissue types (Hong and Saint-Jeannet, 2007; Jaurena et al., 2015), consistent with a direct role of RA in the ectoderm, in the context of the whole embryos we cannot exclude the possibility that Cyp26c1 manipulation may interfere with PPR formation indirectly. To begin addressing this issue, we have performed Cyp26c1MO injections at the eight-cell stage to more specifically target the placode territory (Moody, 1987; Fig. 3L). In these experiments, we observed a similar reduction of *six1* and *foxi1c* expression as seen for two-cell stage injections (Fig. 3M,N), suggesting that RA mediates its activity in the embryonic ectoderm to activate PPR genes. However, the possibility remains that Cyp26c1-regulated RA levels may act indirectly in this context, as

Development (2021) 148, dev193227. doi:10.1242/dev.193227

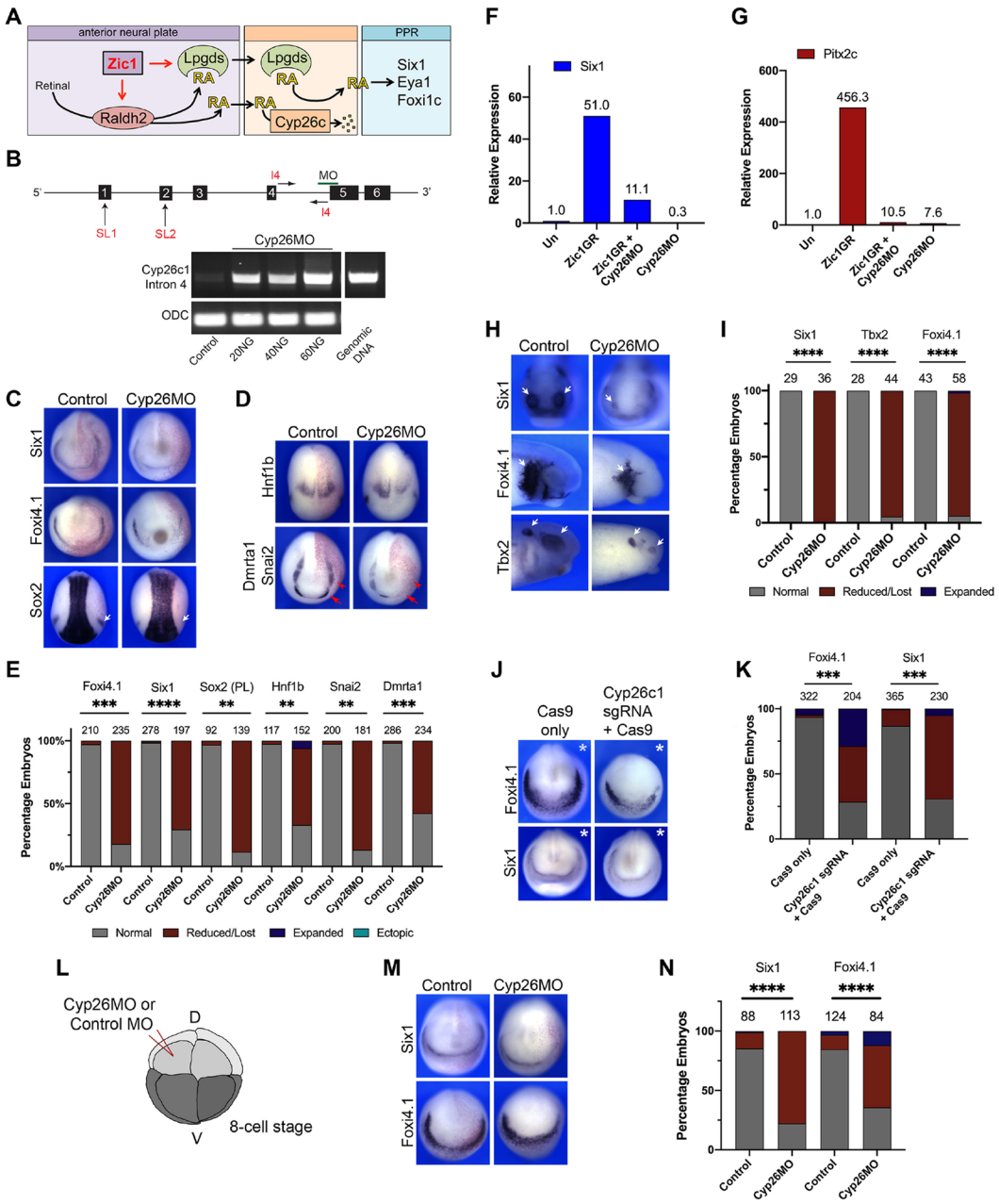

Fig. 3. Cyp26c1 knockdown results in a broad loss of anterior structures. (A) Schematic representation of the working model for PPR specification based on previous work (Jaurena et al., 2015). Anterior neural plate (ANP, purple) expresses Zic1, which induces *raldh2*/*aldh1a2* and *lpgds*/*ptgds*. Raldh2 converts retinal to RA. A putative refractory region (orange) expressing *cyp26c1* lies adjacent, across which RA is transported. At the PPR (blue), RA induces expression of PPR genes *six1*, *eya1* and *foxi1c*/*foxi4.1*. (B, top) Schematic representation of the *cyp26c1* gene structure showing the target site of the splice-blocking morpholino (MO; green bar) and the target sites of sgRNA SL1 and SL2. (B, bottom) RT-PCR analysis showing intron 4 retention in embryos injected with increasing doses of Cyp26c1 morpholino (Cyp26MO). Control indicates uninjected embryos. ODC is shown as loading control and *Xenopus laevis* genomic DNA as a positive control for intron 4 detection. (C,D) *In situ* hybridization for the indicated genes in control and Cyp26MO-injected embryos at stage 15. Injected side (right) showing the lineage tracer Red-Gal. Expression domains of *dmrta1* (red arrows), *snai2* (red arrowheads) and the placode domain of *sox2* (white arrows) are indicated. (E) Quantification of the phenotypes. The number of embryos analyzed is indicated at the top of each bar. *P*-values were calculated using an unpaired *t*-test for the major phenotype, $^{**}P \leq 0.01$, $^{***}P \leq 0.001$, $^{****}P < 0.0001$. (F,G) qRT-PCR analysis of *six1* (F) and *pitx2c* (G) expression in Zic1GR and Zic1GR+Cyp26MO-injected animal cap explants cultured in the presence of dexamethasone. A representative experiment is shown, normalized to ODC. (H) *In situ* hybridization for *six1*, *foxi4.1* and *tbx2* expression in tailbud stage control and bilaterally Cyp26MO-injected embryos. Nasal and epibranchial placodes are visualized using *six1* and *foxi4.1*, respectively (white arrows). The lens and otic vesicle are visualized by *tbx2* (white arrows). Top panels show anterior views, dorsal towards the top. Middle and bottom panels show lateral views, dorsal towards the top. (I) Quantification of the phenotypes. The number of embryos analyzed is indicated at the top of each bar. $^{****}P < 0.0001$, χ^2 test. (J) *In situ* hybridization for *foxi4.1* and *six1* expression in embryos injected with Cas9 alone or with Cyp26c1-sgRNA+Cas9. The injected side is indicated by an asterisk. (K) Quantification of the phenotypes. The number of embryos analyzed for each condition is indicated at the top of each bar. $^{***}P \leq 0.001$, unpaired *t*-test. (L) Schematic representation of eight-cell stage injection. D, dorsal side; V, ventral side. (M) *In situ* hybridization for *six1 and foxi4.1* in control and Cyp26MO-injected embryos at stage 15. Injected side (right) showing the lineage tracer Red-Gal. (N) Quantification of the phenotypes. The number of embryos analyzed is indicated at the top of each bar. $^{****}P < 0.0001$, χ^2 test. Quantification from at least two (I) or three (E,K,N) biological replicates. (F, G) Un, uninjected caps.

Development (2021) 148, dev193227. doi:10.1242/dev.193227

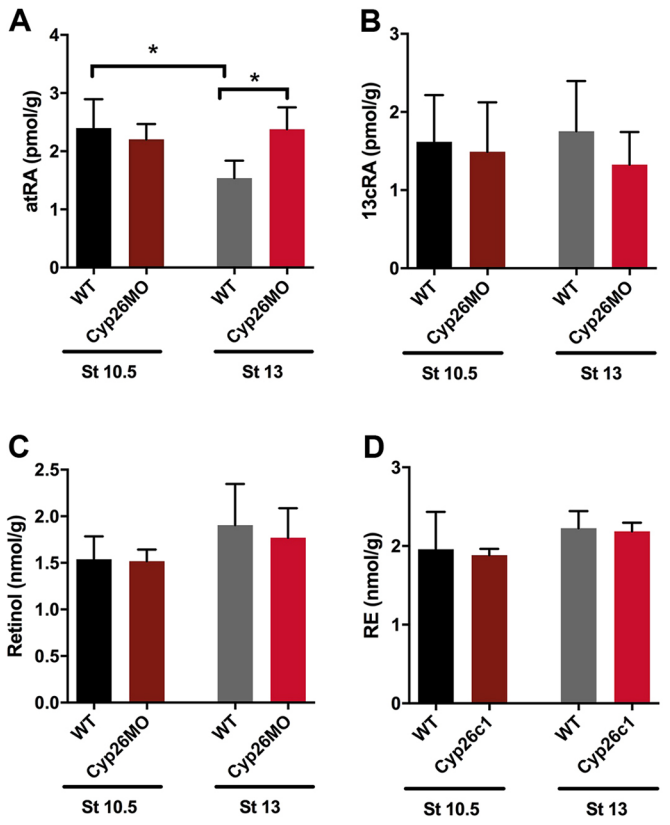

Fig. 4. Measurement of RA levels in wild-type and Cyp26MO-injected embryos. Endogenous retinoids in *Xenopus* embryos of either wild type (WT) or bilaterally injected with Cyp26MO at stages 10.5 and 13. (A) at-RA, (B) 13-*cis*-RA, (C) retinol and (D) RE. Data are for 25 embryos per group and are shown as mean±s.d., n=4 groups per time-point/genotype; *P<0.0247, unpaired t-test. 4-oxo-RA was below the assay limit of detection for groups of 25 embryos.

eight-cell stage injections are likely to affect other ectoderm derivatives (i.e. neural plate and neural crest). Future studies will determine whether Cyp26c1-regulated RA levels directly target the PPR or whether RA acts indirectly by patterning adjacent tissues or regulating another signaling pathway.

To further characterize the phenotype of Cyp26c1 morphant embryos, we analyzed a broader range of ectodermal genes. Interestingly, we found that the expression of the neural crest (*snai2*) and hindbrain (*hnf1b*) genes was also dramatically decreased in morphant embryos (Fig. 3D,E). These results indicate that Cyp26c1 is not only essential for PPR formation, but that its depletion results in a broad loss of anterior structures, consistent with its previously reported function in anterior neural patterning (Tanibe et al., 2008).

Because exposure to excess RA is known to be detrimental to the formation of anterior structures in the embryo (Durston et al., 1989; Abu-Abed et al., 2001; Uehara et al., 2007), we speculate that loss of Cyp26c1 function resulted in excess RA accumulation in the embryo. To test this possibility, we measured by LC-MS/MS endogenous levels of at-RA in wild-type and cyp26c1-depleted embryos at stages 10.5 and 13. Quantitative analyses indicate that at-RA levels are indeed significantly elevated in stage 13 morphant embryos when compared with sibling controls (Fig. 4A), whereas the levels of 13-cis-RA were unchanged (Fig. 4B). The at-RA precursors retinol and retinyl ester (RE) were also unaffected in these embryos (Fig. 4C,D). Taken together, these results establish Cyp26c1 as an important regulator of PPR formation by modulating RA levels anteriorly.

Cyp26a1 is not implicated in PPR formation

Cyp26c1 is one of three enzymes involved in RA degradation. In *Xenopus*, *cyp26c1* and *cyp26a1* are both expressed during gastrulation stages in partially overlapping regions anteriorly (Tanibe et al., 2008), whereas *cyp26b1* is expressed much later in development (Lynch et al., 2011). We observed a mild but consistent expansion of Cyp26a1 upon knockdown of Cyp26c1 (not shown), which was, however, not sufficient to rescue PPR gene expression. Interestingly, morpholino-mediated knockdown of Cyp26a1 (Fig. 5A,B) did not significantly affect *cyp26c1* or *six1* expression (Fig. 5C,D) suggesting that Cyp26a1 has a limited role in PPR formation. Furthermore, unlike *cyp26c1*, *cyp26a1* is not activated by Zic1GR in animal cap explants (Fig. 1E), and is therefore not part of the Zic1-regulated pathway.

PPR patterning by RA

To evaluate the impact of varying RA levels on PPR patterning gene expression, we treated gastrulating embryos with a range of RA doses. We find that increasing doses of RA resulted in strikingly different responses. As previously reported, the *foxi4.1* expression domain was expanded at low doses of RA and reduced at higher doses (Fig. 6A; Jaurena et al., 2015). By contrast, *cyp26c1* and *hnf1b* had an essentially linear expansion with increasing doses of RA, whereas *pitx2c* expression levels steadily decreased with increasing RA (Fig. 6A), suggesting that Pitx2c is acutely sensitive to RA levels. In particular, the two discrete domains of *cyp26c1* expression became indistinguishable or appeared to merge at higher doses of RA, suggesting that at least one domain is RA responsive, consistent with a previous report describing the high sensitivity of the PPR-adjacent region to excess RA (Sive et al., 1990).

In order to distinguish the RA sensitivity of the two *cyp26c1* domains, we investigated changes in *cyp26c1* expression during crucial periods of RA sensitivity for the development of anterior structures (Sive et al., 1990). Embryos at NF stages 10 and 11 were exposed to 1 µM RA, followed by *in situ* hybridization post-neurulation (NF stage 22/23), when the two domains of *cyp26c1* are spatially separated (Fig. 6B). Our results show that the posterior/hindbrain expression domain of *cyp26c1* expanded anteriorly at both stages, in a manner similar to *hnf1b* response (Fig. 5B). By contrast, the expression of *pitx2c* and the PPR-adjacent domain of *cyp26c1* was lost or reduced upon RA treatment (Fig. 6B). These results indicate that the two expression domains of Cyp26c1 are differently regulated and have distinct sensitivity to RA. Taken together, these findings point to differential RA requirement for genes involved in PPR specification, and highlight the need for RA levels to be carefully regulated to pattern the anterior region of the embryo.

Regulation of Cyp26c1 expression by the transcription factor Pitx2c

Our expression data show that *pitx2c* and *cyp26c1* are co-expressed anteriorly in the PPR-adjacent domain, where *pitx2c* temporally precedes *cyp26c1* (Fig. 1I). Moreover, previous work has established that *pitx2* homologs are RA-responsive genes (Matt et al., 2005; Kumar and Duester, 2010; Chawla et al., 2016), suggesting that Pitx2c may participate in PPR formation downstream of Zic1 and upstream of Cyp26c1. In animal cap explants *pitx2c* induction by Zic1 is strongly blocked by disulfiram, a broad inhibitor of RA synthesis (Kitson, 1975; Veverka et al., 1997), in a similar manner as *six1*, confirming that *pitx2c* is activated by RA in this system (Fig. 7A,B; Fig. S5). These data suggest that Zic1, Pitx2c and Cyp26c1 function in the same pathway.

To evaluate a potential role of Pitx2c in the regulation of Cyp26c1, we used a translation-blocking MO (PitxMO1; Fig. 7C) and a splice-

Development (2021) 148, dev193227. doi:10.1242/dev.193227

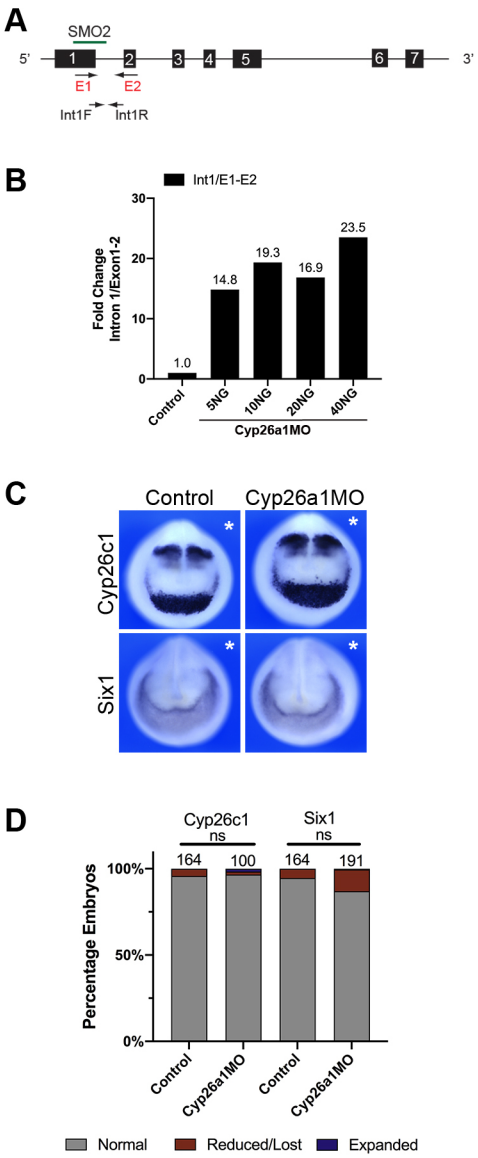

Fig. 5. Cyp26a1 knockdown does not affect *cyp26c1* and *six1* expression. (A) Schematic representation of the *cyp26a1* gene structure, indicating the target site for the splice-blocking morpholino (SMO2; green bar). For representation purposes, the *cyp26a1.L* form is shown; however, the morpholino targets both forms. The primers used to detect intron exclusion are indicated in red (E1, E2) and in black for intron retention (Int1F, Int1R). (B) qRT-PCR analysis of total RNA from embryos bilaterally injected with increasing doses of Cyp26a1 as indicated. The fold change of intron 1 retention over exclusion (exon 1-exon 2) is shown. Values are normalized to ODC prior to calculation of fold change. (C) *In situ* hybridization for *cyp26c1* and *six1* in Cyp26a1SMO2-injected embryos (TexasRed dextran was used as a lineage tracer). The asterisks indicate the injected side. (D) Quantification of the phenotypes in C from at least three biological replicates. The number of embryos analyzed for each condition is indicated at the top of each bar. ns, not significant.

blocking MO (PitxSMO2) targeting the exon 2/intron 2 junction of Pitx2c pre-mRNA (Fig. S6). The specificity of the translation-blocking MO was confirmed by western blot of embryos co-injected with *Pitx2c-Flag* mRNA and PitxMO1 (Fig. 7D). PitxSMO2 disrupts the exon 2/intron 2 splice junction, resulting in a transcript lacking exon 2, as shown by qRT-PCR (Fig. S6). Unilateral injection of either MO resulted in a similar phenotype preferentially reducing the anterior expression domain of *cyp26c1*, and decreasing *six1* expression (Fig. 7E-H). A small number of PitxMO1-injected embryos show expanded *six1* expression (Fig. 7F), which is typically observed in embryos exposed to low doses of RA (Jaurena et al., 2015). Therefore, we speculate that, in these embryos, a partial Pitx2c knockdown may have resulted in an incomplete downregulation of *cyp26c1*, leading to accumulation of RA to levels compatible with *six1* expansion. Altogether, these results suggest that Pitx2c may regulate PPR specification through Cyp26c1. Consistent with this possibility, expression of a hormone inducible version of Pitx2c (Pitx2cGR) in animal cap explants strongly activated Cyp26c1 expression (Fig. 7I; Fig. S7). Interestingly, we found that Pitx2c in this assay was also a potent inducer of fibroblast growth factor 8 (*fgf8*) after 4 h in culture (Fig. 7J; Fig. S7). Fgf8 is an important regulator of PPR formation (Ahrens and Schlosser, 2005), and its expression overlaps anteriorly with Pitx2c (Fig. S8a). In the whole embryos, Pitx2cGR mis-expression induces a posterior shift of the *fgf8* hindbrain expression domain and a reduction of its PPR expression domain (Fig. S8b). This correlates with a massive expansion of *cyp26c1* expression domain. Therefore, the anterior reduction of *fgf8* expression in this context is likely the result of attenuation of endogenous RA signaling via Cyp26c1 upregulation, and the subsequent posteriorization of these embryos (Fig. S8b). Altogether, these results indicate that Pitx2c is activated by Zic1 and induces Cyp26c1, pointing to Pitx2c as a novel regulator of PPR specification upstream of Cyp26c1.

Pitx2c induces Cyp26c1 indirectly via FGF8

Pitx2c is both necessary and sufficient for *cyp26c1* expression, and regulates *fgf8* expression (Fig. 7E-J). To test whether Pitx2c mediates its activity via FGF signaling, we treated animal cap explants expressing Pitx2cGR with the broad FGF receptor inhibitor SU5402 (Mohammadi et al., 1997). This treatment significantly reduced *cyp26c1* induction by Pitx2cGR (Fig. 8A; Fig. S9). These findings were further validated in the whole embryo, where SU5402 treatment severely and selectively reduced *cyp26c1* expression in the PPR-adjacent domain, while the hindbrain domain was largely unaffected (Fig. 8B,C). The *pitx2c* expression domain was unperturbed in these embryos; however, the PPR expression domain of *foxi4.1* was also significantly reduced (Fig. 8B,C). The requirement for FGF signaling was further confirmed using a MO to specifically interfere with *fgf8a* (Fgf8aMO; Fletcher et al., 2006). Upon *fgf8a* knockdown, both *cyp26c1* and *foxi4.1* were significantly reduced, whereas *pitx2c* expression was largely unchanged (Fig. 8D,E). The hindbrain expression domain of *cyp26c1* was also affected in Ffg8MO-injected embryos. This is likely due to differences in the treatment regimens used for the drug versus the MO. SU5402 was applied at gastrulation (stage 11), whereas Fgf8MO was injected at the two-cell stage, therefore affecting Fgf8 function at an earlier time-point than SU5402. Sustained Fgf8 knockdown is presumably more broadly detrimental to embryonic development. Taken together, these results demonstrate that Pitx2c participates in PPR formation by regulating *cyp26c1* expression anteriorly in an FGF-dependent manner.

DISCUSSION

The crucial role of morphogens in patterning the embryo is well established. However, the mechanistic details of how these gradients are distributed and interpreted by target cells remain unclear. Our previous work (Jaurena et al., 2015) showed the existence of an anterior source of RA activated by Zic1 and crucial for PPR induction. However, this observation left largely unresolved the mechanism by which RA signaling activate PPR genes in a spatially restricted domain, adjacent to the Zic1-generated source of RA. In this study, we have dissected this mechanism, demonstrating that the

Development (2021) 148, dev193227. doi:10.1242/dev.193227

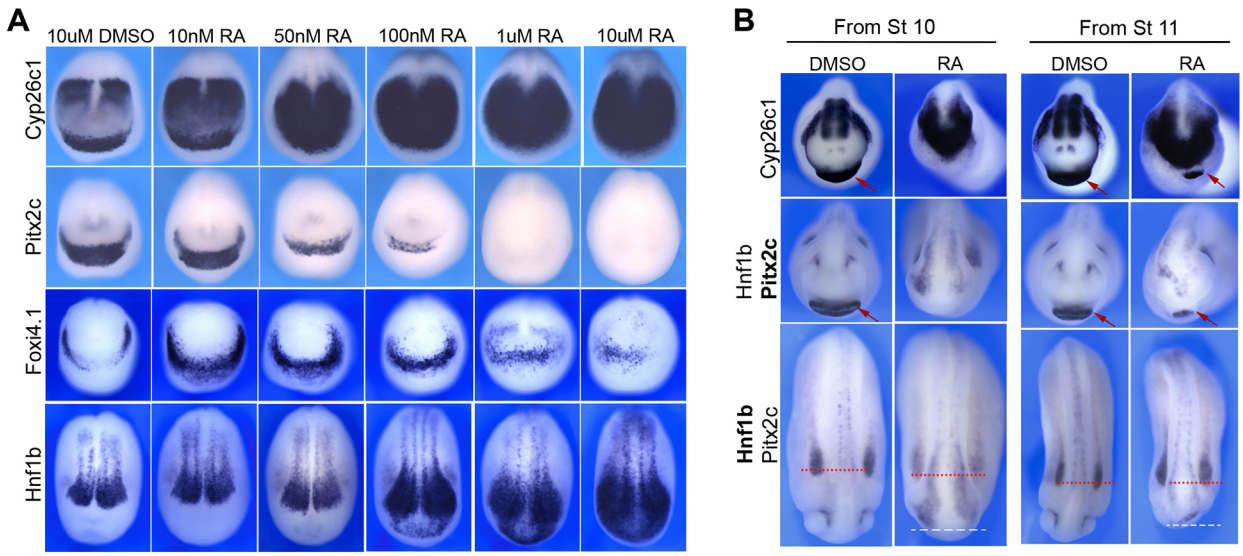

Fig. 6. RA sensitivity and dose response of PPR-related genes. (A) *In situ* hybridization for *cyp26c1*, *pitx2c*, *foxi4.1* and *hnf1b* expression on stage 15 embryos treated with either 1 µM DMSO with increasing doses of RA as shown. (B) *In situ* hybridization analysis of stage 22 embryos treated with either 1 µM DMSO or 1 µM RA at stages 10 and 11. For double *in situ* hybridization (middle and bottom rows), the gene being assessed is indicated with bold letters, *pitx2c* (middle rows) and *hnf1b* (bottom rows). Red arrows indicate the position of the cement gland region. The red dotted lines indicate the anterior boundary of *hnf1b* expression under normal conditions, which expands anteriorly under conditions of excess RA (1 µM, white dashed line). (A,B) The phenotypes are fully penetrant; *n*>45 embryos per conditions from three biological replicates. (A,B) All images show anterior views with dorsal towards top, except for *hnf1b*, where dorsal views are presented with anterior towards bottom.

production of RA is only one step in the regulatory cascade leading to PPR formation, and that two Zic1 targets, the transcription factor Pitx2c and the RA degrading enzyme Cyp26c1, are essential effectors that act in concert to modulate RA levels anteriorly for proper PPR gene expression. By direct measurement of endogenous retinoids in the embryo using LC-MS/MS, we show that Cyp26c1 controls RA levels to promote PPR gene expression in a spatially restricted domain. Therefore, it is not the mere production of RA that is crucial to initiate a PPR development program, but rather its tight regulation by the Cyp26c1 enzyme, which is activated in the vicinity of the PPR by Pitx2c in a FGF-dependent manner. Thus, we propose that Zic1 activation at the ANP serves to create a program of RA containment and regulation through Cyp26c1 and Pitx2c cooperation to promote PPR specification in a spatially restricted domain (Fig. 9A). Under conditions of excess RA, owing to Cyp26c1 knockdown or exposure to exogenous RA, *pitx2c* and *pitx2c/cyp26c1* are downregulated, respectively, thus preventing modulation of RA levels necessary for PPR gene activation (Fig. 9B). Although our experiments indicate an essential role for RA in establishing the PPR, future studies will help determine whether Cyp26c1-regulated RA levels control PPR formation directly or indirectly through the patterning of adjacent tissues or the regulation of other signaling pathways.

Cyp26c1 is essential for PPR formation

Cyp26c1 was first identified in a microarray screen for Zic1 targets during PPR formation (Jaurena et al., 2015). Knockdown of Cyp26c1 using either MO or CRISPR/Cas9 resulted in a drastic reduction of PPR and neural crest gene expression. By direct measurement of endogenous RA levels in Cyp26-depleted embryos (NF stage 13), we demonstrated that this phenotype was due to excess RA accumulation (Fig. 4A), thereby confirming that Cyp26c1 is required to maintain low RA levels in the anterior regions of the embryo for PPR gene expression. Interestingly, the levels of 4-oxo-RA detected in embryos at all stages were higher than those observed for at-RA, suggesting that 4-oxo-RA could be the major species of retinoid in *Xenopus* (Blumberg et al., 1996). In fact, Cyp26c1 has been shown to be efficient in clearing 4-oxo-RA into further polar metabolites (Zhong et al., 2018); therefore, *cyp26c1*-mediated degradation is required in this region, regardless of the retinoid species present. This will be further investigated in future work by comparing at-RA and 4-oxo-RA for their capacity to regulate PPR gene expression.

Late stage embryos lacking Cyp26c1 showed a marked truncation of head structures (Fig. 3H,I) and did not survive past stage 30. This is consistent with reports in mice, where the loss of both Cyp26c1 and Cyp26a1 was severely detrimental to neural tube closure and resulted in truncation of anterior structures (Uehara et al., 2007). The co-requirement of Cyp26a1 in mice is not surprising as typically a high level of redundancy is observed in mammalian gene families and not as much in *Xenopus*. Although Cyp26c1 and Cyp26a1 are both expressed in partially overlapping regions anteriorly, MO-mediated knockdown of Cyp26a1 did not affect *cyp26c1* or *six1* expression, ruling out the possibility of a reciprocal compensation during PPR formation (Fig. 5).

To evaluate the potential mechanism(s) underlying the loss of PPR genes in Cyp26c1-depleted embryos, we have analyzed whether these cells: (1) had activated alternate ectoderm fates by looking at *sox2* (neural plate) and *keratin* (epidermis) expression by qRT-PCR; (2) were targeted for cell death, detected using TUNEL staining; or (3) had impaired proliferation, determined by pHH3 staining. We used both animal cap explants expressing Zic1 (1) and whole embryos (2 and 3). We found no significant changes in *sox2* and *keratin* expression in animal cap explants expressing Zic1 upon Cyp26c1 knockdown, and the rate of cell death and proliferation were unaffected in Cyp26c1 morphant embryos (data not shown and Fig. S10, respectively). Future studies will determine whether these cells remain in an undifferentiated/pluripotent state or have activated non-ectodermal cell fates.

Development (2021) 148, dev193227. doi:10.1242/dev.193227

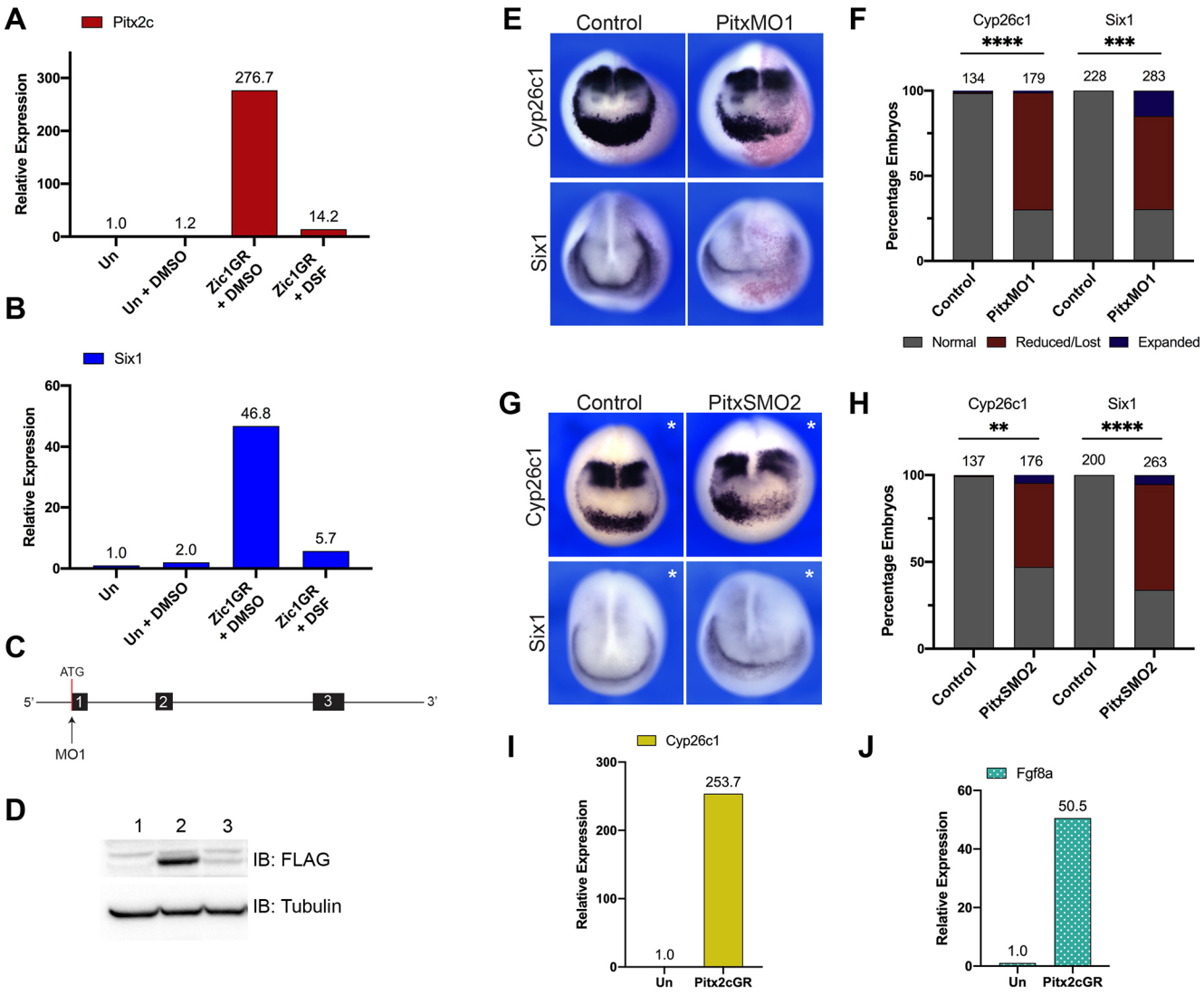

Fig. 7. Regulation of Cyp26c1 expression by the transcription factor Pitx2c. (A,B) qRT-PCR analysis of *pitx2c* (A) and *six1* (B) expression in animal cap explants injected with Zic1GR mRNA and cultured for 8 h in the presence of dexamethasone with or without disulfiram (DSF; 100 µM). Values are normalized to ODC. A representative experiment is shown. (C) Schematic representation of the *pitx2c* gene structure, indicating the target site for the translation-blocking (MO1; black arrow) morpholino. (D) Western blot analysis of protein lysates from control embryos (lane 1), *Pitx2c-FLAG* mRNA-injected embryos (lane 2) and *Pitx2c-FLAG* mRNA co-injected with 20 ng of PitxMO1 (lane 3). Tubulin is shown as a loading control (bottom panel). (E,G) *In situ* hybridization for *cyp26c1* and *six1* expression in PitxMO1- (E) and PitxSMO2-injected embryos (G). Red-Gal (E) or RFP (G) were used as a lineage tracer. The asterisks indicate the injected side. (I,J) qRT-PCR analysis for *cyp26c1* (I) and *fgf8a* (J) expression in animal cap explants injected with Pitx2cGR mRNA and cultured in the presence of dexamethasone. The values are normalized to ODC. *cyp26c1* expression was assessed after 8 h in culture, while *fgf8a* expression was evaluated after 4 h in culture. (F,H) Quantification of the phenotypes from E and G, respectively, from at least three biological replicates. The total number of embryos is indicated at the top of each bar. *P*-values for the association between morpholino injection and level of gene expression were calculated using an unpaired *t*-test for the major phenotype, $^{**}P \leq 0.01$, $^{***}P \leq 0.001$, $^{****}P < 0.0001$ in F,H. (E,G) All images show anterior views with dorsal to the top.

PPR patterning through local gradient generation

The catabolism of RA mediated by Cyp26 enzymes is known to be crucial to establish discrete domains of RA signaling in the embryo by preventing signal spreading and directing propagation, as well as regulating RA levels within a domain (Bok et al., 2011; da Silva and Cepko, 2017; Ono et al., 2020). These adjacent and complementary domains of production and degradation within the embryo are crucial for patterning sensory tissues, and disruptions of these domains can have dramatic consequences on subsequent fate specification (for a detailed review, see Dubey et al. (2018).

Our results reveal the existence of such juxtaposed domains in the embryonic head of *Xenopus* embryos: the RA-producing ANP that expresses Raldh2/Aldh1a2 (Jaurena et al., 2015) and the RA-degrading domain defined by the anterior expression domain of Cyp26c1 that partially overlaps with the PPR. Thus, the precursor region for all cranial placodes also employs this very precise mechanism of RA modulation seen in specification of complex sensory tissues. This supports the view that, in addition to its posteriorizing activity during development (Villanueva et al., 2002; Kudoh et al., 2002), independent pockets of highly regulated RA signaling are also used throughout development for tissue specification.

Regulation of Cyp26c1 expression anteriorly

Examination of previously identified Zic1 targets (Bae et al., 2014; Jaurena et al., 2015) for their expression in regions adjacent to the

Development (2021) 148, dev193227. doi:10.1242/dev.193227

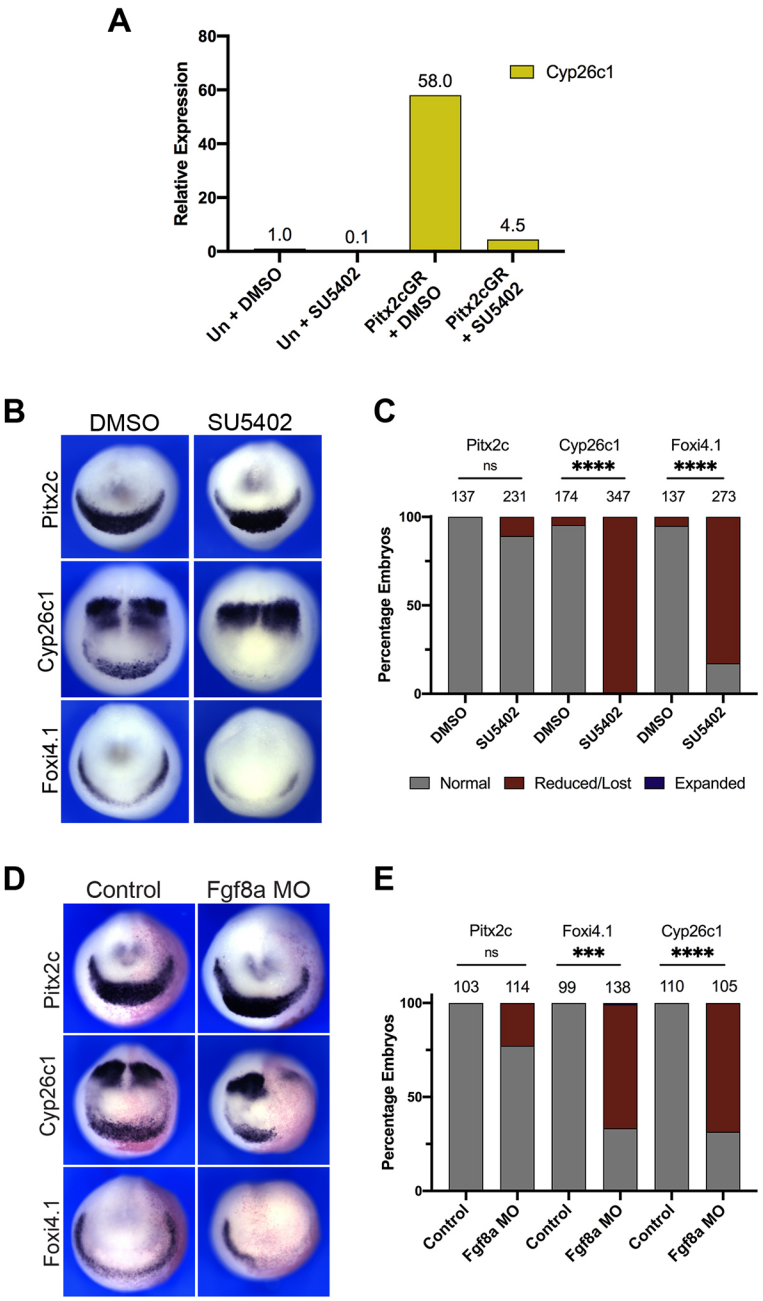

Fig. 8. FGF signaling is required for *cyp26c1* expression and PPR formation. (A) qRT-PCR analysis of *cyp26c1* expression in animal cap explants injected with Pitx2cGR mRNA and cultured for 8 h in the presence of dexamethasone with DMSO or SU5402 (25 µM). Values are normalized to ODC. A representative experiment is shown. (B) *In situ* hybridization for *pitx2c*, *cyp26c1* and *foxi4.1* on NF stage 15 embryos treated with DMSO or SU5402. (D) *In situ* hybridization for *pitx2c*, *cyp26c1* and *foxi4.1* expression in control NF stage 15 embryos and embryos injected with Fgf8aMO. Injected side with Red-Gal is on the right. (C,E) Quantification of the phenotypes from B and D, respectively, from at least three biological replicates. Total embryos analyzed are indicated at the top of each bar. *P* values were calculated using an unpaired *t*-test for the major phenotype (reduced *cyp26c1* expression in the anterior domain or reduced *foxi4.1* expression), ***$P \leq 0.001$, ****$P < 0.0001$; ns, not significant (C,D). (A,B) All images show anterior views with dorsal towards the top.

PPR yielded Pitx2c as a potential regulator of Cyp26c1. Pitx2c is a transcription factor that controls left-right asymmetry, and is a known RA target (Liu et al., 2001). Perturbations in Pitx2c function have been known to result in craniofacial, ocular and tooth defects in mice (Liu et al., 2003). In *Xenopus*, *pitx2c* is co-expressed with *cyp26c1* in the PPR-adjacent domain, where it precedes *cyp26c1* (Fig. 1I). We show that *pitx2c* is activated by Zic1 in an RA-dependent manner, (Fig. 7A) and is necessary (Fig. 7E-H) and sufficient (Fig. 7I) for *cyp26c1* expression. Interestingly, *pitx2c* expression is also dependent on Cyp26c1 function in animal cap explants (Fig. 3G) and in the embryo (Fig. S11), suggesting that Cyp26c1 is also required to dampen RA levels and maintain *pitx2c* expression in this region. The RA dose response experiments further support a model where Cyp26c1 participates in a feedback loop to maintain low RA levels within the PPR-adjacent domain for proper expression of *pitx2c*, a gene acutely sensitive to excess RA (Fig. 6A).

In addition to *pitx2c*, we find evidence that exogenous RA is capable of expanding *cyp26c1* expression (Fig. 6A). Further analysis revealed that this expansion is largely contributed by the hindbrain expression domain of *cyp26c1*, which behaves like *hnf1b*, a known RA-responsive gene (Gere-Becker et al., 2018). By contrast, the *cyp26c1* PPR-adjacent domain displays significantly greater sensitivity and is abolished under excess RA (Fig. 5B), similar to the PPR genes *foxi4.1* and *pitx2c* (Fig. 6A). These observations indicate that *cyp26c1* hindbrain and PPR-adjacent expression domains are independently regulated, with contrasting RA dependence.

Regulation of Cyp26c1 expression by Pitx2c depends on FGF signaling

RA and FGF signaling often interact during embryogenesis (Hernandez et al., 2004; Shiotsugu et al., 2004; Cunningham et al.,

Development (2021) 148, dev193227. doi:10.1242/dev.193227

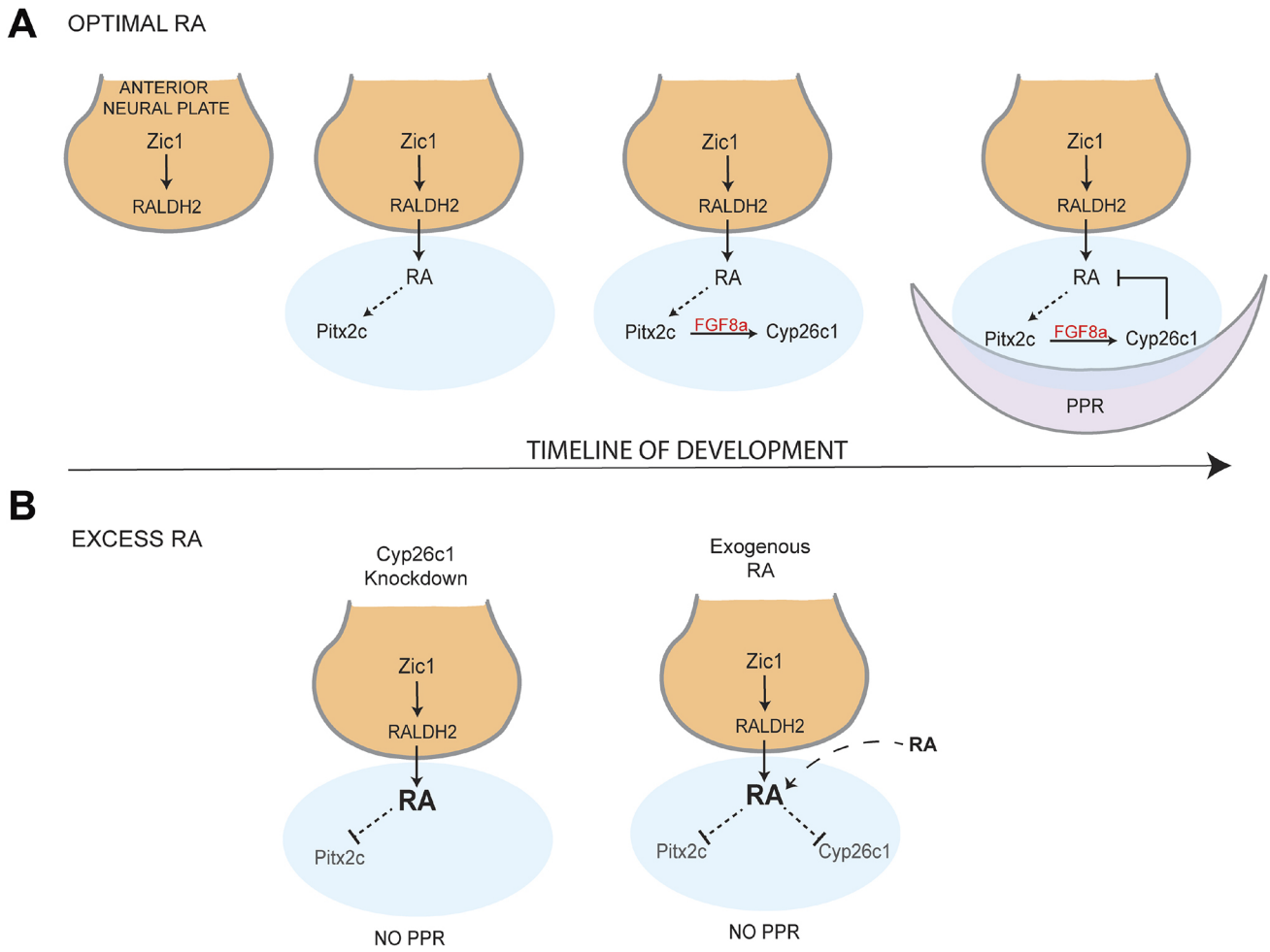

Fig. 9. Model for Zic1-regulated PPR formation. (A) Under normal conditions (optimal RA levels), at the end of gastrulation, Zic1 is expressed in the prospective anterior neural plate (orange), where it activates the expression of *raldh2*/*adh1a2*. RA synthesized by *raldh2*/*adh1a2* is transported to the adjacent PPR-adjacent region (blue) where it activates *pitx2c* expression. Subsequently, Pitx2c induces the expression of *cyp26c1* in the same domain via activation of Fgf8a. Cyp26c1 in turn maintains RA at low levels for sustained *pitx2c* expression and elicits the activation of PPR-specific genes. (B) Under conditions of excess RA, upon Cyp26c1 knockdown (left panel) or on exposure to exogenous RA (right panel), *pitx2c* and *pitx2c*/*cyp26c1* are downregulated, respectively, preventing the modulation of RA to levels necessary for PPR gene activation.

2013), and FGF8 is expressed in PPR-adjacent regions, both in *Xenopus laevis* (Fletcher et al., 2006; Hong et al., 2008) and in *Xenopus tropicalis* (Lea et al., 2009). Pitx2c is a potent inducer of FGF8a in animal cap explants (Fig. 7J), which can be detected as early as 4 h, suggesting that Fgf8 expression precedes Cyp26c1 induction when the pathway is first activated. Interference with FGF signaling in the embryo results in specific loss of cyp26c1 expression in the PPR-adjacent domain, reduction of *foxi4.1* expression at the PPR (Fig. 8A-C), without affecting *pitx2c* expression domain. This suggests that Pitx2c activates *cyp26c1* expression anteriorly through upregulation of FGF8a. This is consistent with other reports showing that Cyp26 enzymes are activated by FGF signaling, as seen for Cyp26c1 in the chick otic placode and retina (da Silva and Cepko, 2017; Yang et al., 2013), and for Cyp26a1 in the paraxial mesoderm (Moreno and Kintner, 2004). These findings point to Pitx2c as a key factor integrating both RA and FGF signaling to pattern the PPR.

Overall, our observations strongly support a model where Zic1, in an RA-dependent manner, activates *pitx2c*, which in turn is crucial for regulating *cyp26c1* expression indirectly through FGF signaling (Fig. 9). The Pitx2c-expressing PPR-adjacent region serves as an important regulatory domain at early neurula stage for RA containment and regulation through Cyp26c1 activation that operates within a specific temporal window to promote PPR specification in a spatially restricted domain. Computational and experimental data in zebrafish have shown that Cyp26a1 is regulated by both RA and FGF to generate a robust RA gradient in the embryo (White et al., 2007; Casci, 2008). We find a similar setup for *Xenopus* PPR specification, where both RA and FGF interact to regulate Cyp26c1 expression presumably to generate a local gradient of RA free of fluctuations.

MATERIALS AND METHODS

Plasmids, constructs and oligonucleotides

Xenopus laevis Zic1GR and Pitx2cGR constructs are hormone-inducible versions of Zic1 and Pitx2c, generated by fusing the human glucocorticoid receptor (GR) ligand-binding domain (Kolm and Sive, 1995) to the coding region of Pitx2c and Zic1 in a pCS2+ backbone (Hong and Saint-Jeannet, 2007). Cyp26c1-pBSK was a gift from Dr Makoto Asashima (University of Tokyo, Japan) (Tanibe et al., 2008). The Pitx2c-FLAG construct was generated by addition of 1x FLAG tag (DYKDDDDK) at the C-terminus of Pitx2c in the pCS2+ backbone using the following reverse primer: 5′-AGTCTAGACTTGTCGTCATCGTCTTTGTAGTCCACGGGTCTG-3′. Zic1GR, Pitx2c-Flag, Pitx2cGR, β-galactosidase and red fluorescent protein

Development (2021) 148, dev193227. doi:10.1242/dev.193227

(RFP) mRNAs were synthesized using the Message mMachine SP6 and T7 Transcription kits (Ambion; SP6, AM1340; T7, AM1344) and purified using the RNAeasy MinElute Cleanup Kit (Qiagen, 74204). Zic1 (Zic1-MO) (Sato et al., 2005), Fgf8a (Fgf8aMO) (Fletcher et al., 2006), Cyp26c1 (Cyp26MO: GATTCCTGAAAGCCAAGAACATACG) and Pitx2c (PitxMO1: TTTCA-TAGAGTTCATGGAGGATGGT; PitxSMO2: AACCAGACCTGAAGG-AGGCAGAATA) morpholino antisense oligonucleotides (MO) were purchased from GeneTools. A standard control morpholino (CoMO; CCTCTTACCTCAGTTACAATTTATA) was used as control. The efficiency of knockdown by the Cyp26c1 splice-blocking MO (Cyp26c1-MO) was validated by RT-PCR on injected embryos (Fig. 3B) using the following primers spanning intron 4, (I4): forward, 5′-CTATACATATGA-GGTTTCAGCCCTG-3′; reverse: 5′-CTGAAAGCCAAGAACATACGTG-3′. To validate knockdown by PitxSMO2, RT-PCR on injected embryos was performed using primers in exon 2 (E2; 5′-AATCGCAGTGTGGACCAAT-3′) and exon 3 (E3; 5′-TGGTTCCTCTCCCTCTTTCT-3′) (Fig. S6).

Embryos, injections, treatments and animal cap explant culture

Xenopus laevis embryos were staged according to Nieuwkoop and Faber (NF) (Nieuwkoop and Faber, 1967) and raised in 0.1× Normal Amphibian Medium (NAM) (Slack and Forman, 1980). All experiments in this study were conducted in accordance with the guidelines of the Guide for the Care and Use of Laboratory Animals of the National Institutes of Health. All protocols requiring *Xenopus* were approved by the Institutional Animal Care and Use Committee of New York University under animal protocol IA16-00052. In microinjection experiments, embryos were injected in one blastomere at the two-cell stage (NF stage 2) or in one animal dorsal blastomere at the eight-cell stage (NF stage 4), collected at NF stage 15 and processed for *in situ* hybridization (ISH). The injection solutions consisted of 40-60 ng of MO and 0.5 ng of β-galactosidase mRNA as a lineage tracer. Embryos injected with CoMO were used as controls. In experiments involving retinoic acid (all-trans RA, Sigma-Aldrich, R2625) and SU5402 (Tocris, 3300) treatments, stock solutions were prepared in DMSO (dimethylsulfoxide). NF stage 11 embryos were incubated in RA diluted in 0.1× NAM (0.01 µM, 0.05 µM, 0.1 µM, 1 µM and 10 µM) or 25 µM SU5402 in 0.1× NAM. Sibling embryos were treated with 10 µM or 25 µM DMSO as controls.

Animal cap explant experiments were conducted by injecting one blastomere at the two-cell stage in the animal pole region with 250 pg Zic1GR or 500 pg Pitx2cGR mRNA. For the experiments described in Fig. 3E, Zic1GR and Cyp26c1-MO were injected in opposite blastomeres due to the non-cell autonomous role of Zic1 in PPR gene induction (Jaurena et al., 2015). The explants were dissected at the blastula stage (NF stage 9) and cultured in 0.5× NAM with 10 µM dexamethasone (Sigma-Aldrich, D1756) for 8 h at 24°C unless otherwise noted, then collected and immediately stored at −80°C. For some experiments, 100 µM disulfiram (tetraethylthiuram disulfide, Sigma-Aldrich, 86720) and 25 µM SU5402 were added to the incubation medium. All experiments were performed on at least three independent batches of embryos (obtained from three separate females). On average, 50 embryos per injection and per marker were used in whole-embryo experiments, and 12-15 animal caps per experiment were used in animal cap explant assays.

CRISPR/Cas9 mutagenesis

Two single guide RNAs (sgRNAs) (SL1, 5′-GGCTGCTTCTCACCAGC-TC-3′; SL2, 5′-GCCGGTTATTCGAGTGACA-3′) were used and generated as described by Nakayama et al. (2013). Conserved regions between the L and S form of Cyp26c1 were chosen as target regions for SL1 and SL2. sgRNAs were synthesized using the MegaShortScript Kit (Ambion, AM1354M) and purified using MEGAClear kit (Ambion, AM1908). Cas9 recombinant protein was purchased from PNA Bio (CP01-20). For CRISPR-Cas9 injections, a mix of 1 ng total of sgRNAs, 2 ng of Cas9 protein and Texas Red Dextran (Molecular Probes, D1863) was used. Injections were performed unilaterally at the two-cell stage, and embryos injected with Cas9 protein alone were used as controls. Efficacy of sgRNAs was determined by direct sequencing of PCR amplicons (DSP) assay, as described previously (Nakayama et al., 2014; Fig. S4). Sequence alignment was performed using Geneious Prime.

In situ hybridization

In situ hybridization was carried out as previously described (Harland, 1991; Jaurena et al., 2015; Saint-Jeannet, 2017). Briefly, embryos were collected at the indicated stage and fixed in MEMFA (0.1 M MOPS, 2 mM EGTA, 1 mM $MgSO_4$ and 3.7% formaldehyde). If β-galactosidase mRNA was used as a tracer, Red-Gal (Research Organics, C40040) staining was performed prior to *in situ* hybridization. If the tracer used was RFP or TexasRed Dextran, prior to fixation the embryos were first screened for fluorescence signal either in the left or right half of the embryo, sorted, and then fixed and processed independently for *in situ* hybridization.

Whole-mount *in situ* hybridization (Saint-Jeannet, 2017) was carried out in 4 ml glass vials on a standard bench top nutator. *Zic1* (Mizuseki et al., 1998), *Foxi4.1* (Schlosser and Ahrens, 2004; Pohl et al., 2002), *Six1* (Pandur and Moody, 2000), *Snai2* (Mayor et al., 1995), *Dmrta1* (Huang et al., 2005), *Hnf1b* (Demartis et al., 1994), *Sox2* (Mizuseki et al., 1998), *Pitx2c* (Jeong et al., 2014), *Cyp26c1* (Tanibe et al., 2008) and *Fgf8a* (Christen and Slack, 1997) digoxygenin (DIG)- or fluorescein isothiocyanate (FITC)-labeled antisense RNA probes were synthesized using the Genius Kit (Roche, 1175025). The hybridization step was performed overnight at 60°C. For detection of RNA probes, an anti-DIG antibody conjugated to alkaline phosphatase (Roche, 11093274910; 1:2000 dilution) was used overnight at 4°C. Excess antibody was removed through several successive washes and the chromogenic reaction performed overnight at room temperature in BM purple (Roche, 11442074001). The embryos were subsequently bleached in 10% hydrogen peroxide in methanol for 48 h. For double *in situ* hybridization, DIG- and FITC-labeled probes were co-incubated and detected sequentially with anti-FITC antibody conjugated to alkaline phosphatase (Roche, 11426338910; 1:10,000 dilution) and anti-DIG alkaline phosphatase conjugated antibodies, respectively. The FITC-labeled probe was visualized using Magenta Phosphate (5-bromo-6-chloro-3-indolyl phosphate; Biosynth, B7452) for several days. After inactivation by treatment with glycine (0.1 M, pH 2.2) for 30 min, the DIG-labeled probe was visualized with 4-toluidine salt (BCIP; Roche, 11383221001) until a robust signal was achieved. The two-color reactions were followed by bleaching of embryos in 10% hydrogen peroxide in PBS for a few hours, and imaged in 1× PBS.

TUNEL and pHH3 staining

TUNEL staining was performed according to the protocol described by Hensey and Gautier (1998). Briefly, Cyp26c1MO-injected albino embryos were fixed in MEMFA, rehydrated in PBT and washed in TdT buffer (Roche). End labeling was subsequently performed at room temperature in TdT buffer containing 0.5 µM DIG-dUTP and 150 U/ml TdT (Roche). Embryos were then washed at 65°C in PBS/1 mM EDTA, and DIG was detected using anti-DIG Fab fragments conjugated to alkaline phosphatase (Roche; 1:2000). For phosphohistone H3 (pHH3) detection (Saka and Smith, 2001), embryos were incubated successively in an anti-pHH3 antibody (Upstate Biotechnology, 06-570; 1 µg/ml) and anti-rabbit IgG secondary conjugated to alkaline phosphatase (ThermoFisher Scientific, G-21079; 1:1000). The chromogenic reaction was performed using NBT/BCIP (Roche). Sf3b4MO-injected albinos embryos were used as a positive control (Devotta et al., 2016).

Extraction and quantification of retinoids

Batches of 130 (wild-type analysis) and 25 (wild type versus Cyp26MO analysis) embryos at NF stages 9, 10.5 and 13 collected from at least three different females were immediately frozen in liquid nitrogen. The samples were stored in −80°C until processed. Embryos were homogenized in 1 ml saline. Extraction of retinoids was performed under yellow lights using a two-step liquid-liquid extraction that has been described in detail previously, using 4,4-dimethyl-RA as an internal standard for RA and retinyl acetate as an internal standard for retinol and total retinyl ester (Jones et al., 2015; Kane et al., 2005, 2008b; Kane and Napoli, 2010). For the extraction of retinoids, 3 ml of 0.025 M KOH in ethanol was added to embryo homogenates followed by addition of 10 ml hexane to the aqueous ethanol phase. The samples were vortexed and centrifuged for 1 to 3 min at ∼1000 ***g*** in a Dynac centrifuge (Becton Dickinson) to facilitate phase separation and pellet precipitated protein. The hexane (top) phase containing

Development (2021) 148, dev193227. doi:10.1242/dev.193227

nonpolar retinoids (retinol and RE) was removed. 4 M HCl (180 µl) was added to the remaining aqueous ethanol phase, samples were vortexed and then polar retinoids (RA, 4-oxo-RA) were removed by extraction with a second 10 ml aliquot of hexane as described above. Organic hexane phases were evaporated under nitrogen while heating at ∼30°C in a water bath (model N-EVAP 112, Organomation Associates). All samples were resuspended in 60 µl acetonitrile. Only glass containers, pipettes and syringes were used to handle retinoids.

Levels of RA were determined by liquid chromatography-multistage tandem mass spectrometry (LC-MRM^3), which is an LC-MS/MS method using two distinct fragmentation events for enhanced selectivity (Jones et al., 2015). RA was measured using a Shimadzu Prominence UFLC XR liquid chromatography system coupled to an AB Sciex 6500+ QTRAP hybrid triple quadrupole mass spectrometer using atmospheric pressure chemical ionization (APCI) operated in positive ion mode as previously described (Jones et al., 2015). For the LC separation, the column temperature was controlled at 25°C, the auto-sampler was maintained at 10°C and the injection volume was typically 20 µl. All separations were performed using an Ascentis Express RP-Amide guard cartridge column (Supelco, 50×2.1 mm, 2.7 µm) coupled to an Ascentis Express RP-Amide analytical column (Supelco, 100×2.1 mm, 2.7 µm). Mobile phase A consisted of 0.1% formic acid in water; mobile phase B consisted of 0.1% formic acid in acetonitrile. Endogenously occurring retinoid isomers, including all-trans-retinoic acid (RA), 9-*cis* retinoic acid, 13-*cis* retinoic acid and 9,13-di-*cis* retinoic acid, were resolved using a gradient separation at a flow rate of 0.4 ml/min with the following gradient: 0-1 min, 60% B; 1-7 min, ramp to 95% B; 7-9 min, hold at 95% B; 9-9.5 min, ramp to 10% B; 9.5-10.5 min, hold at 10% B; 10.5-11 min, ramp to 95% B; 11-12.5 min, hold at 95% B; 12.5-13 min, ramp to 60% B; 13-15 min, re-equilibrate at 60% B. The APCI source conditions and MRM^3 detection parameters were as follows: curtain gas, 15; collision gas, low; nebulizer current, 3; temperature, 325; ion source gas, 55; declustering potential, 56; entrance potential, 12; collision energy, 1; excitation energy, 0.1; excitation time, 25; ion trap fill time, 125. The MRM^3 transition for RA was *m/z* 301.1→*m/z* 205.1→*m/z* 159.1 and for 4,4-dimethyl RA was *m/z* 329.2→*m/z* 151.2→*m/z* 100.0.

Levels of all-trans-4-oxo-RA (4-oxo-RA) were determined by liquid chromatography-tandem mass spectrometry (LC-MS/MS) method using method modified from Kane and Napoli (2010). 4-oxo-RA was measured using a Shimadzu Prominence UFLC XR liquid chromatography system coupled to an AB Sciex 6500+ QTRAP hybrid triple quadrupole mass spectrometer using atmospheric pressure chemical ionization (APCI) operated in positive ion mode. For the LC separation, the column temperature was controlled at 25°C, the autosampler was maintained at 10°C and the injection volume was typically 20 µl. All separations were performed using an Ascentis Express RP-Amide guard cartridge column (Supelco, 50×2.1 mm, 2.7 µm) coupled to an Ascentis Express RP-Amide analytical column (Supelco, 100×2.1 mm, 2.7 µm). Mobile phase A consisted of 0.1% formic acid in water; mobile phase B consisted of 0.1% formic acid in acetonitrile. Endogenously occurring retinoid isomers including all-trans-4-oxo-retinoic acid (4-oxo-RA) and 13-*cis*-4-oxo-retinoic acid were resolved using a gradient separation at a flow rate of 0.4 ml/min with the following gradient: 0-3 min, 40% B; 3-16 min, ramp to 95% B; 16-19 min, hold at 95% B; 19-19.5 min, ramp to 10% B; 19.5-20.5 min, hold at 10% B; 20.5-21 min, ramp to 95% B; 21-22.5 min, hold at 95% B; 22.5-23 min, ramp to 40% B; 23-25 min, re-equilibrate at 40% B. The APCI source conditions and MRM detection parameters were as follows: curtain gas, 20; collision gas, medium; nebulizer current, 3; temperature, 325; gas 1, 35; gas 2, 30; declustering potential, 20; entrance potential, 4; collision energy, 15; collision exit potential, 23; dwell time, 150 ms. The MRM transition for 4-oxo-RA (and 13-*cis*-4-oxo-retinoic acid) was *m/z* 315.1→m/z 297.1 and for internal standards 4-oxo-RA-d3 was *m/z* 318.1→m/z 300.0 and for internal standard 13-*cis*-4-oxo-retinoic acid-d6 was *m/z* 321.1→m/z 303.1.

Levels of retinol and total retinyl esters (RE) were quantified via HPLC-UV according to previously published methodology (Kane and Napoli, 2010; Kane et al., 2008a). Retinol and RE were resolved by reverse-phase chromatography (Zorbax SB-C18, 4.6×100 mm, 3.5 µm) on a Waters Acquity UPLC H-class system and were quantified by UV absorbance at 325 nm. Analytes were separated at 1 ml/min with 11% water/89% acetonitrile/0.1% formic acid for 9 min, followed by a linear gradient over 2 min to 100% acetonitrile. Then 100% acetonitrile was maintained for 2 min, followed by a linear gradient over 2 min to 5% acetonitrile/1,2-dichloroethane. Final conditions were held for 2 min before returning to initial conditions. Injection volume was 30 µl for all samples.

The amount of retinoic acid (RA), retinol (ROL) and total retinyl ester (RE) was normalized per g of tissue for embryo analyses. Average weights of embryos were similar among groups and on average (mean±s.d.) were as follows: 130 embryos (as in Fig. 2) were 283.4±23.1 mg and 25 embryos (as in Fig. 4) were 57.1±7.5 mg.

Western blot analysis

Embryos were injected at the two-cell stage with 2.5 ng of *Xenopus* Pitx2c-Flag mRNA alone or with increasing doses of PitxMO1 and collected at stage 13. Pools of 10 embryos were homogenized in lysis buffer (1% Triton X-100, 5 mM EDTA in 0.1x NAM) containing Halt Protease Inhibitor Cocktail (78429, ThermoFisher Scientific). Lysis was performed for 30 min on ice with occasional vortexing. After two consecutive centrifugations (to eliminate lipids), 10 µl of the concentrated lysate was resolved on a 4-12% NuPAGE Bis-Tris gel and transferred onto a PVDF membrane using the iBlot system (Invitrogen). Blots were subsequently incubated overnight with the monoclonal anti-Flag M2 primary antibody (Sigma Aldrich, F3165; 1:1000 dilution). The blots were then washed and incubated with anti-mouse IgG coupled to horseradish peroxidase (Santa Cruz Biotechnology; 1:10,000). Peroxidase activity was detected with the Western Blotting Luminol Reagent (sc-2048, Santa Cruz Biotechnology) and imaged on a ChemiDoc MP Biorad gel documentation system. Membranes were stripped using Restore Western Blot Stripping Buffer (21062 ThermoFisher Scientific) according to the manufacturer's recommendations and incubated with anti α-tubulin antibody (Sigma Aldrich, T9026; 1:500 dilution).

qRT-PCR analysis

Total RNA was extracted from 12-15 animal cap explants using the RNeasy Micro kit (Qiagen, 74004). To eliminate genomic DNA, on-column digestion was performed with RNase-free DNase I for 15 min at room temp. The amount of RNA isolated was quantified using a Nanodrop spectrophotometer (Nanodrop Technologies) and 10 ng total RNA was used per reaction. qRT-PCR was performed using the One Step RT-PCR kit (Applied Bioystems, 4388869, 4389988). The mean Ct value for each biological replicate was computed from four technical replicates. The primers used for qRT-PCR are listed in Table S1.

Imaging

Images of *in situ* hybridization-processed embryos were captured using a dual light-fluorescence Leica M165 Stereomicroscope using the same exposure and magnification settings for each marker in the experiment. Representative images of the dominant phenotype were captured and the image panels were composed using Adobe Photoshop.

Statistical analysis

Experiments were conducted in embryos from three or more female *Xenopus* for biological replicates. No prior analysis was carried out to determine sample size. Injected embryos were compared with both the uninjected side of each embryo, and with uninjected and CoMO-injected embryos for expression of gene of interest. One of the following phenotypes was assigned to each embryo: normal, lost or reduced, expanded, or ectopic. For RA/inhibitor treated embryos, the treated embryos were compared with DMSO-treated controls and assigned phenotypes as above. The data from all biological replicates were pooled for statistical analysis. In all graphs, control groups included both uninjected and CoMO-injected embryos. Significance testing for whole-mount *in situ* hybridization experiments was performed using the χ^2 test for multiple outcomes (such as normal and expanded gene expression) and an unpaired, two-tailed *t*-test for major outcome. The unpaired, two-tailed

t-test was also used for analysis of LC-MS/MS experiments. $P<0.05$ was considered significant and analyses were performed using GraphPad Prism 8. For qRT-PCR experiments, a representative experiment is shown in the main results, and the remaining two biological replicates are provided in Figs S1, S3, S5, S7 and S9.

Acknowledgements
We thank members of the Saint-Jeannet laboratory for technical assistance and helpful discussions. We thank Jonathan Cooney for assistance with the Pitx2c-GR construct, Dr Nadège Gouignard for reagents, Dr Makoto Asashima for the Cyp26c1 plasmid and Dr Young-Hoon Lee for the Pitx2c plasmid. This work benefited from the support of Xenbase (http://www.xenbase.org/ - RRID: SCR_003280) and the National Xenopus Resource (http://mbl.edu/xenopus/ - RRID:SCR_013731). The sgRNAs used in this study were first tested at a Genome Editing Workshop at the National Xenopus Resource.

Competing interests
The authors declare no competing or financial interests.

Author contributions
Conceptualization: A.D., J.-P.S.-J.; Methodology: A.D., J.Y., T.L., M.A.K., J.-P.S.-J.; Formal analysis: A.D., J.Y., T.L., M.A.K., J.-P.S.-J.; Investigation: A.D., J.Y., T.L., J.-P.S.-J.; Writing - original draft: A.D., J.-P.S.-J.; Writing - review & editing: A.D., M.A.K., J.-P.S.-J.; Supervision: M.K., J.-P.S.-J.; Project administration: J.-P.S.-J.; Funding acquisition: M.K., J.-P.S.-J.

Funding
This work was supported by grants from the National Institutes of Health (R01-DE025806 to J.-P.S.-J., F32-DE027599 to A.D. and R01HD077260 to M.A.K.). This work was also supported in part by the University of Maryland School of Pharmacy Mass Spectrometry Center (SOP1841-IQB2014). Deposited in PMC for release after 12 months.

Supplementary information
Supplementary information available online at
https://dev.biologists.org/lookup/doi/10.1242/dev.193227.supplemental

References
Abu-Abed, S., Dollé, P., Metzger, D., Beckett, B., Chambon, P. and Petkovich, M. (2001). The retinoic acid-metabolizing enzyme, CYP26A1, is essential for normal hindbrain patterning, vertebral identity, and development of posterior structures. *Genes Dev.* **15**, 226-240. doi:10.1101/gad.855001

Ahrens, K. and Schlosser, G. (2005). Tissues and signals involved in the induction of placodal Six1 expression in *Xenopus laevis*. *Dev. Biol.* **288**, 40-59. doi:10.1016/j.ydbio.2005.07.022

Bae, C.-J., Park, B.-Y., Lee, Y.-H., Tobias, J. W., Hong, C.-S. and Saint-Jeannet, J.-P. (2014). Identification of Pax3 and Zic1 targets in the developing neural crest. *Dev. Biol.* **386**, 473-483. doi:10.1016/j.ydbio.2013.12.011

Baker, C. V. H. and Bronner-Fraser, M. (2001). Vertebrate cranial placodes I. Embryonic induction. *Dev. Biol.* **232**, 1-61. doi:10.1006/dbio.2001.0156

Baron, J. M., Heise, R., Blaner, W. S., Neis, M., Joussen, S., Dreuw, A., Marquardt, Y., Saurat, J.-H., Merk, H. F., Bickers, D. R. et al. (2005). Retinoic acid and its 4-Oxo metabolites are functionally active in human skin cells in vitro. *J. Investig. Dermatol.* **125**, 143-153. doi:10.1111/j.0022-202X.2005.23791.x

Blumberg, B., Bolado, J., Derguini, F., Craig, A. G., Moreno, T. A., Chakravarti, D., Heyman, R. A., Buck, J. and Evans, R. M. (1996). Novel retinoic acid receptor ligands in Xenopus embryos. *Proc. Natl. Acad. Sci. USA* **93**, 4873-4878. doi:10.1073/pnas.93.10.4873

Bok, J., Raft, S., Kong, K.-A., Koo, S. K., Dräger, U. C. and Wu, D. K. (2011). Transient retinoic acid signaling confers anterior-posterior polarity to the inner ear. *Proc. Natl. Acad. Sci. USA* **108**, 161-166. doi:10.1073/pnas.1010547108

Casci, T. (2008). Retinoic acid passes the morphogen test. *Nat. Rev. Genet.* **9**, 7. doi:10.1038/nrg2293

Chawla, B., Schley, E., Williams, A. L. and Bohnsack, B. L. (2016). Retinoic acid and Pitx2 regulate early neural crest survival and migration in craniofacial and ocular development. *Birth Defects Res. B Dev. Reprod. Toxicol.* **107**, 126-135. doi:10.1002/bdrb.21177

Christen, B. and Slack, J. M. W. (1997). FGF-8Is associated with anteroposterior patterning and limb regeneration inXenopus. *Dev. Biol.* **192**, 455-466. doi:10.1006/dbio.1997.8732

Cunningham, T. J., Zhao, X., Sandell, L. L., Evans, S. M., Trainor, P. A. and Duester, G. (2013). Antagonism between retinoic acid and fibroblast growth factor signaling during Limb development. *Cell Rep.* **3**, 1503-1511. doi:10.1016/j.celrep.2013.03.036

da Silva, S. and Cepko, C. L. (2017). Fgf8 expression and degradation of retinoic acid are required for patterning a high-acuity area in the retina. *Dev. Cell* **42**, 68-81.e6. doi:10.1016/j.devcel.2017.05.024

Demartis, A., Maffei, M., Vignali, R., Barsacchi, G. and DE Simone, V. (1994). Cloning and developmental expression of LFB3/HNF1β transcription factor in Xenopus laevis. *Mech. Dev.* **47**, 19-28. doi:10.1016/0925-4773(94)90092-2

Devotta, A., Juraver-Geslin, H., Gonzalez, J. A., Hong, C. S. and Saint-Jeannet, J. P. (2016). Sf3b4-depleted Xenopus embryos: a model to study the pathogenesis of craniofacial defects in Nager syndrome. *Dev. Biol.* **415**, 371-382. doi:10.1016/j.ydbio.2016.02.010

Dubey, A., Rose, R. E., Jones, D. R. and Saint-Jeannet, J.-P. (2018). Generating retinoic acid gradients by local degradation during craniofacial development: One cell's cue is another cell's poison. *Genesis* **56**, e23091. doi:10.1002/dvg.23091

Duester, G. (2008). Retinoic acid synthesis and signaling during early organogenesis. *Cell,* **134**, 921-931. doi:10.1016/j.cell.2008.09.002

Durston, A. J., Timmermans, J. P. M., Hage, W. J., Hendriks, H. F. J., de Vries, N. J., Heideveld, M. and Nieuwkoop, P. D. (1989). Retinoic acid causes an anteroposterior transformation in the developing central nervous system. *Nature* **340**, 140-144. doi:10.1038/340140a0

Fletcher, R. B., Baker, J. C. and Harland, R. M. (2006). *FGF8* spliceforms mediate early mesoderm and posterior neural tissue formation in *Xenopus*. *Development* **133**, 1703-1714. doi:10.1242/dev.02342

Gere-Becker, M. B., Pommerenke, C., Lingner, T. and Pieler, T. (2018). Retinoic acid-induced expression of Hnf1b and Fzd4 is required for pancreas development in Xenopus laevis. *Development* **145**, dev161372. doi:10.1242/dev.161372

Grocott, T., Tambalo, M. and Streit, A. (2012). The peripheral sensory nervous system in the vertebrate head: A gene regulatory perspective. *Dev. Biol.* **370**, 3-23. doi:10.1016/j.ydbio.2012.06.028

Harland, R. M. (1991). Appendix G: in situ hybridization: an improved whole-mount method for xenopus embryos. In *Methods in Cell Biology* (ed. B. K. Kay and H. B. Peng), pp. 685-695. Academic Press.

Hensey, C. and Gautier, J. (1998). Programmed cell death during Xenopus development: a spatio-temporal analysis. *Dev. Biol.* **203**, 36-48. doi:10.1006/dbio.1998.9028

Hernandez, R. E., Rikhof, H. A., Bachmann, R. and Moens, C. B. (2004). *vhnf1* integrates global RA patterning and local FGF signals to direct posterior hindbrain development in zebrafish. *Development* **131**, 4511-4520. doi:10.1242/dev.01297

Hong, C.-S. and Saint-Jeannet, J.-P. (2007). The activity of Pax3 and Zic1 regulates three distinct cell fates at the neural plate border. *Mol. Biol. Cell* **18**, 2192-2202. doi:10.1091/mbc.e06-11-1047

Hong, C.-S., Park, B.-Y. and Saint-Jeannet, J.-P. (2008). Fgf8a induces neural crest indirectly through the activation of Wnt8 in the paraxial mesoderm. *Development* **135**, 3903-3910. doi:10.1242/dev.026229

Huang, X., Hong, C.-S., O'donnell, M. and Saint-Jeannet, J.-P. (2005). The doublesex-related gene, XDmrt4, is required for neurogenesis in the olfactory system. *Proc. Natl. Acad. Sci. USA* **102**, 11349-11354. doi:10.1073/pnas.0505106102

Janesick, A., Shiotsugu, J., Taketani, M. and Blumberg, B. (2012). RIPPLY3 is a retinoic acid-inducible repressor required for setting the borders of the pre-placodal ectoderm. *Development* **139**, 1213-1224. doi:10.1242/dev.071456

Jaurena, M. B., Juraver-Geslin, H., Devotta, A. and Saint-Jeannet, J.-P. (2015). Zic1 controls placode progenitor formation non-cell autonomously by regulating retinoic acid production and transport. *Nat. Commun.* **6**, 7476-7476. doi:10.1038/ncomms8476

Jeong, Y.-H., Park, B.-K., Saint-Jeannet, J.-P. and Lee, Y.-H. (2014). Developmental expression of Pitx2c in Xenopus trigeminal and profundal placodes. *Int. J. Dev. Biol.* **58**, 701-704. doi:10.1387/ijdb.140254js

Jones, J. W., Pierzchalski, K., Yu, J. and Kane, M. A. (2015). Use of fast HPLC multiple reaction monitoring cubed for endogenous retinoic acid quantification in complex matrices. *Anal. Chem.* **87**, 3222-3230. doi:10.1021/ac504597q

Kane, M. A. and Napoli, J. L. (2010). Quantification of endogenous retinoids. In *Retinoids: Methods and Protocols* (ed. H. Sun and G. H. Travis), pp. 1-54. Totowa, NJ: Humana Press.

Kane, M. A., Chen, N., Sparks, S. and Napoli, J. L. (2005). Quantification of endogenous retinoic acid in limited biological samples by LC/MS/MS. *Biochem. J.* **388**, 363-369. doi:10.1042/BJ20041867

Kane, M. A., Folias, A. E. and Napoli, J. L. (2008a). HPLC/UV quantitation of retinal, retinol, and retinyl esters in serum and tissues. *Anal. Biochem.* **378**, 71-79. doi:10.1016/j.ab.2008.03.038

Kane, M. A., Folias, A. E., Wang, C. and Napoli, J. L. (2008b). Quantitative Profiling of Endogenous Retinoic Acid in Vivo and in Vitro by Tandem Mass Spectrometry. *Anal. Chem.* **80**, 1702-1708. doi:10.1021/ac702030f

Kitson, T. M. (1975). The effect of disulfiram on the aldehyde dehydrogenases of sheep liver. *Biochem. J.* **151**, 407-412. doi:10.1042/bj1510407

Kolm, P. J. and Sive, H. L. (1995). Efficient hormone-inducible protein function in Xenopus laevis. *Dev. Biol.* **171**, 267-272. doi:10.1006/dbio.1995.1279

Kudoh, T., Wilson, S. W. and Dawid, I. B. (2002). Distinct roles for Fgf, Wnt and retinoic acid in posteriorizing the neural ectoderm. *Development* **129**, 4335-4346.

Kumar, S. and Duester, G. (2010). Retinoic acid signaling in perioptic mesenchyme represses Wnt signaling via induction of Pitx2 and Dkk2. *Dev. Biol.* **340**, 67-74. doi:10.1016/j.ydbio.2010.01.027
le Douarin, N. (1986). Cell line segregation during peripheral nervous system ontogeny. *Science* **231**, 1515-1522. doi:10.1126/science.3952494
Lea, R., Papalopulu, N., Amaya, E. and Dorey, K. (2009). Temporal and spatial expression of FGF ligands and receptors during Xenopus development. *Dev. Dyn.* **238**, 1467-1479. doi:10.1002/dvdy.21913
Li, Y., Manaligod, J. M. and Weeks, D. L. (2010). EYA1 mutations associated with the branchio-oto-renal syndrome result in defective otic development in Xenopus laevis. *Biol. Cell* **102**, 277-292. doi:10.1042/BC20090098
Liu, C., Liu, W., Lu, M.-F., Brown, N. A. and Martin, J. F. (2001). Regulation of left-right asymmetry by thresholds of Pitx2c activity. *Development* **128**, 2039-2048.
Liu, W., Selever, J., Lu, M.-F. and Martin, J. F. (2003). Genetic dissection of *Pitx2* in craniofacial development uncovers new functions in branchial arch morphogenesis, late aspects of tooth morphogenesis and cell migration. *Development* **130**, 6375-6385. doi:10.1242/dev.00849
Lynch, J., Mcewan, J. and Beck, C. W. (2011). Analysis of the expression of retinoic acid metabolising genes during Xenopus laevis organogenesis. *Gene Expression Patterns* **11**, 112-117. doi:10.1016/j.gep.2010.10.003
Matt, N., Dupé, V., Garnier, J.-M., Dennefeld, C., Chambon, P., Mark, M. and Ghyselinck, N. B. (2005). Retinoic acid-dependent eye morphogenesis is orchestrated by neural crest cells. *Development* **132**, 4789-4800. doi:10.1242/dev.02031
Mayor, R., Morgan, R. and Sargent, M. G. (1995). Induction of the prospective neural crest of Xenopus. *Development* **121**, 767-777.
Mizuseki, K., Kishi, M., Matsui, M., Nakanishi, S. and Sasai, Y. (1998). Xenopus Zic-related-1 and Sox-2, two factors induced by chordin, have distinct activities in the initiation of neural induction. *Development* **125**, 579-587.
Mohammadi, M., Mcmahon, G., Sun, L., Tang, C., Hirth, P., Yeh, B. K., Hubbard, S. R. and Schlessinger, J. (1997). Structures of the tyrosine kinase domain of fibroblast growth factor receptor in complex with inhibitors. *Science* **276**, 955-960. doi:10.1126/science.276.5314.955
Moody, S. A. (1987). Fates of the blastomeres of the 16-cell-stage *Xenopus* embryo. *Dev. Biol.* **119**, 560-578. doi:10.1016/0012-1606(87)90059-5
Moody, S. A. and Lamantia, A.-S. (2015). Transcriptional regulation of cranial sensory placode development. *Curr. Top. Dev. Biol.* **111**, 301-350. doi:10.1016/bs.ctdb.2014.11.009
Moreno, T. A. and Kintner, C. (2004). Regulation of segmental patterning by retinoic acid signaling during Xenopus Somitogenesis. *Dev. Cell* **6**, 205-218. doi:10.1016/S1534-5807(04)00026-7
Nakayama, T., Fish, M. B., Fisher, M., Oomen-Hajagos, J., Thomsen, G. H. and Grainger, R. M. (2013). Simple and efficient CRISPR/Cas9-mediated targeted mutagenesis in Xenopus tropicalis. *Genesis* **51**, 835-843. doi:10.1002/dvg.22720
Nakayama, T., Blitz, I. L., Fish, M. B., Odeleye, A. O., Manohar, S., Cho, K. W. Y. and Grainger, R. M. (2014). Cas9-based genome editing in Xenopus tropicalis. *Methods Enzymol.* **546**, 355-375. doi:10.1016/B978-0-12-801185-0.00017-9
Nieuwkoop, P. D. and Faber, J. (1967). *Normal Table of Xenopus laevis (Daudin)*. North Holland, Amsterdam: Garland Publishing
Ono, K., Keller, J., LÓPEZ Ramírez, O., GONZÁLEZ Garrido, A., Zobeiri, O. A., Chang, H. H. V., Vijayakumar, S., Ayiotis, A., Duester, G., DELLA Santina, C. C. et al. (2020). Retinoic acid degradation shapes zonal development of vestibular organs and sensitivity to transient linear accelerations. *Nat. Commun.* **11**, 63. doi:10.1038/s41467-019-13710-4
Pandur, P. D. and Moody, S. A. (2000). Xenopus Six1 gene is expressed in neurogenic cranial placodes and maintained in the differentiating lateral lines. *Mech. Dev.* **96**, 253-257. doi:10.1016/S0925-4773(00)00396-8
Paschaki, M., Cammas, L., Muta, Y., Matsuoka, Y., Mak, S.-S., Rataj-Baniowska, M., Fraulob, V., Dollé, P. and Ladher, R. K. (2013). Retinoic acid regulates olfactory progenitor cell fate and differentiation. *Neural Dev.* **8**, 13. doi:10.1186/1749-8104-8-13
Pijnappel, W. W. M., Hendriks, H. F. J., Folkers, G. E., van den Brink, C. E., Dekker, E. J., Edelenbosch, C., van der Saag, P. T. and Durston, A. J. (1993). The retinoid ligand 4-oxo-retinoic acid is a highly active modulator of positional specification. *Nature* **366**, 340-344. doi:10.1038/366340a0
Pohl, B. S., Knöchel, S., Dillinger, K. and Knöchel, W. (2002). Sequence and expression of FoxB2 (XFD-5) and FoxI1c (XFD-10) in Xenopus embryogenesis. *Mech. Dev.* **117**, 283-287. doi:10.1016/S0925-4773(02)00184-3
Ruf, R. G., Xu, P.-X., Silvius, D., Otto, E. A., Beekmann, F., Muerb, U. T., Kumar, S., Neuhaus, T. J., Kemper, M. J., Raymond, R. M.Jr et al. (2004). SIX1 mutations cause branchio-oto-renal syndrome by disruption of EYA1-SIX1-DNA complexes. *Proc. Natl. Acad. Sci. USA* **101**, 8090-8095. doi:10.1073/pnas.0308475101
Saint-Jeannet, J.-P. (2017). Whole-mount in situ hybridization of xenopus embryos. *Cold Spring Harb. Protoc.* **2017**, pdb.prot097287. doi:10.1101/pdb.prot097287
Saint-Jeannet, J.-P. and Moody, S. A. (2014). Establishing the pre-placodal region and breaking it into placodes with distinct identities. *Dev. Biol.* **389**, 13-27. doi:10.1016/j.ydbio.2014.02.011
Saka, Y. and Smith, J. C. (2001). Spatial and temporal patterns of cell division during early Xenopus embryogenesis. *Dev. Biol.* **229**, 307-318. doi:10.1006/dbio.2000.0101
Sato, T., Sasai, N. and Sasai, Y. (2005). Neural crest determination by co-activation of Pax3 and Zic1 genes in Xenopus ectoderm. *Development* **132**, 2355-2363. doi:10.1242/dev.01823
Schlosser, G. (2006). Induction and specification of cranial placodes. *Dev. Biol.* **294**, 303-351. doi:10.1016/j.ydbio.2006.03.009
Schlosser, G. and Ahrens, K. (2004). Molecular anatomy of placode development in Xenopus laevis. *Dev. Biol.* **271**, 439-466. doi:10.1016/j.ydbio.2004.04.013
Schönberger, J., Wang, L., Shin, J. T., Kim, S. D., Depreux, F. F. S., Zhu, H., Zon, L., Pizard, A., Kim, J. B., Macrae, C. A. et al. (2005). Mutation in the transcriptional coactivator EYA4 causes dilated cardiomyopathy and sensorineural hearing loss. *Nat. Genet.* **37**, 418-422. doi:10.1038/ng1527
Shiotsugu, J., Katsuyama, Y., Arima, K., Baxter, A., Koide, T., Song, J., Chandraratna, R. A. S. and Blumberg, B. (2004). Multiple points of interaction between retinoic acid and FGF signaling during embryonic axis formation. *Development* **131**, 2653-2667. doi:10.1242/dev.01129
Sive, H. L., Draper, B. W., Harland, R. M. and Weintraub, H. (1990). Identification of a retinoic acid-sensitive period during primary axis formation in Xenopus laevis. *Genes Dev.* **4**, 932-942. doi:10.1101/gad.4.6.932
Slack, J. M. W. and Forman, D. (1980). An interaction between dorsal and ventral regions of the marginal zone in early amphibian embryos. *J. Embryol. Exp. Morphol.* **56**, 283-299.
Takabatake, Y., Takabatake, T. and Takeshima, K. (2000). Conserved and divergent expression of T-box genes Tbx2-Tbx5 in Xenopus. *Mech. Dev.* **91**, 433-437. doi:10.1016/S0925-4773(99)00329-9
Tanibe, M., Michiue, T., Yukita, A., Danno, H., Ikuzawa, M., Ishiura, S. and Asashima, M. (2008). Retinoic acid metabolizing factor xCyp26c is specifically expressed in neuroectoderm and regulates anterior neural patterning in Xenopus laevis. *Int. J. Dev. Biol.* **52**, 893-901. doi:10.1387/ijdb.082683mt
Uehara, M., Yashiro, K., Mamiya, S., Nishino, J., Chambon, P., Dolle, P. and Sakai, Y. (2007). CYP26A1 and CYP26C1 cooperatively regulate anterior–posterior patterning of the developing brain and the production of migratory cranial neural crest cells in the mouse. *Dev. Biol.* **302**, 399-411. doi:10.1016/j.ydbio.2006.09.045
Veverka, K. A., Johnson, K. L., Mays, D. C., Lipsky, J. J. and Naylor, S. (1997). Inhibition of aldehyde dehydrogenase by disulfiram and its metabolite methyl diethylthiocarbamoyl-sulfoxide. *Biochem. Pharmacol.* **53**, 511-518. doi:10.1016/S0006-2952(96)00767-8
Villanueva, S., Glavic, A., Ruiz, P. and Mayor, R. (2002). Posteriorization by Fgf, Wnt, and retinoic acid is required for neural crest induction. *Dev. Biol.* **241**, 289-301. doi:10.1006/dbio.2001.0485
White, R. J., Nie, Q., Lander, A. D. and Schilling, T. F. (2007). Complex Regulation of cyp26a1 creates a robust retinoic acid gradient in the zebrafish embryo. *PLoS Biol.* **5**, e304. doi:10.1371/journal.pbio.0050304
Xu, P.-X., Zheng, W., Laclef, C., Maire, P., Maas, R. L., Peters, H. and Xu, X. (2002). *Eya1* is required for the morphogenesis of mammalian thymus, parathyroid and thyroid. *Development* **129**, 3033-3044.
Yang, L., O'neill, P., Martin, K., Maass, J. C., Vassilev, V., Ladher, R. and Groves, A. K. (2013). Analysis of FGF-dependent and FGF-independent pathways in Otic placode induction. *PLoS ONE* **8**, e55011. doi:10.1371/journal.pone.0055011
Yu, S.-B., Umair, Z., Kumar, S., Lee, U., Lee, S.-H., Kim, J.-I., Kim, S., Park, J.-B., Lee, J.-Y. and Kim, J. (2016). xCyp26c induced by inhibition of BMP signaling is involved in anterior-posterior neural patterning of Xenopus laevis. *Mol. Cells* **39**, 352-357. doi:10.14348/molcells.2016.0006
Zhong, G., Ortiz, D., Zelter, A., Nath, A. and Isoherranen, N. (2018). CYP26C1 is a hydroxylase of multiple active retinoids and interacts with cellular retinoic acid binding proteins. *Mol. Pharmacol.* **93**, 489-503. doi:10.1124/mol.117.111039

SUPPLEMENTARY DATA

Figure S1: Developmental RT-PCR of genes involved in PPR specification

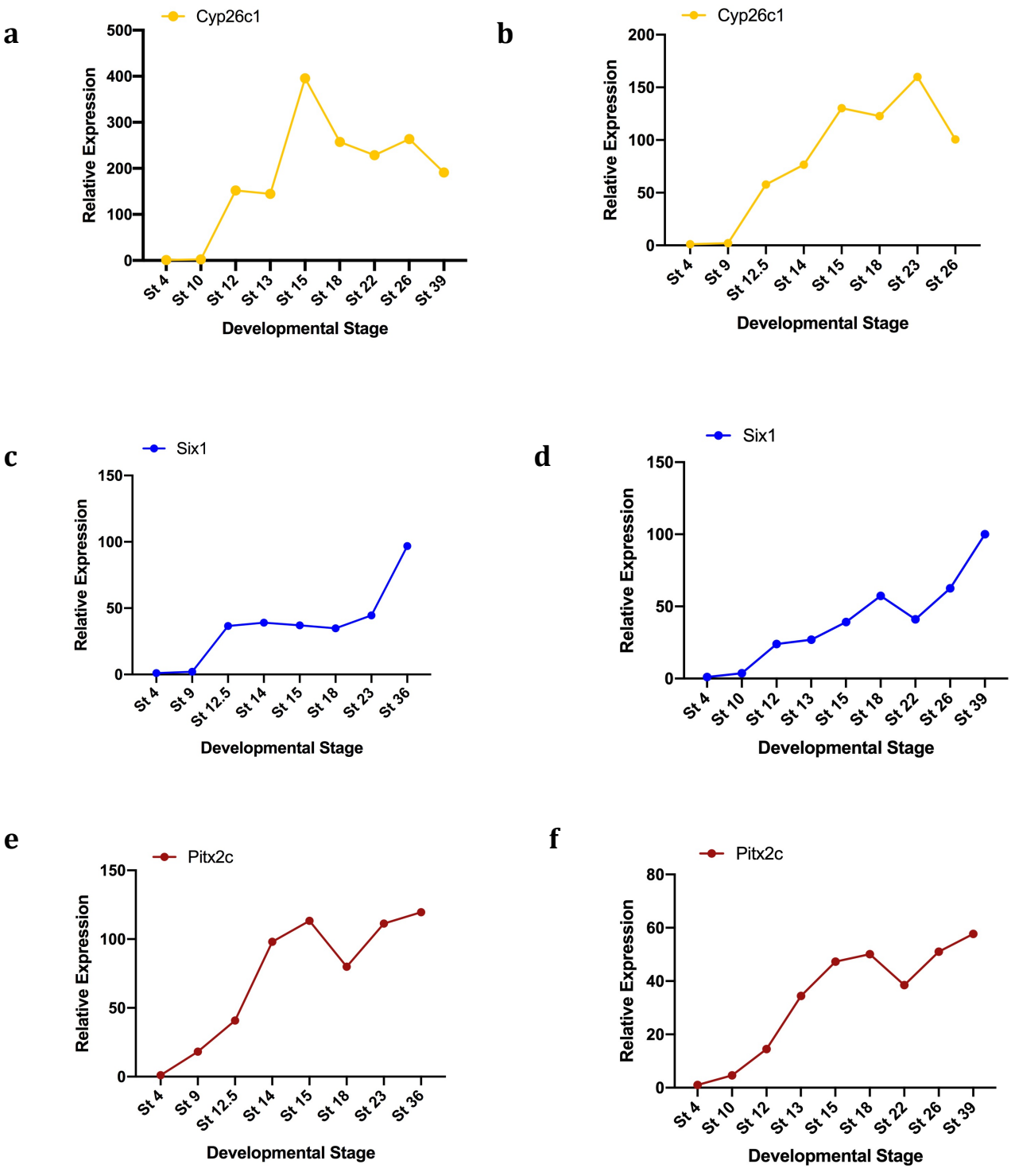

Figure S1: Developmental qRT-PCR expression profile *cyp26c1* (a,b), *six1* (c, d) and *pitx2c* (e, f) in two biological replicates (a, c, e and b, d, f) of WT *Xenopus* embryos. NF stages are indicated on x-axis, values are normalized to ODC.

Figure S2: Endogenous retinoid detection in the whole embryo by LC-MS/MS

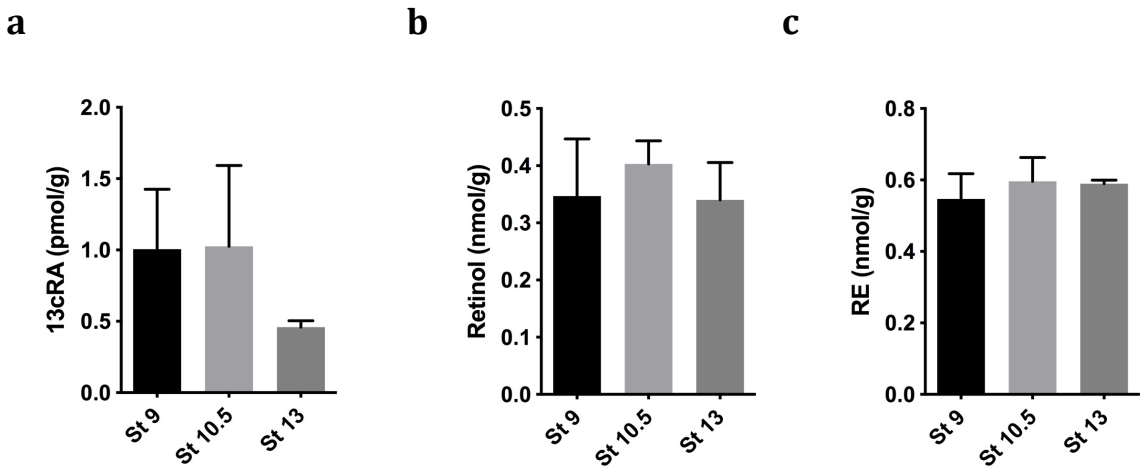

Figure S2: Endogenous retinoids in the whole embryo at stage 9, 10.5 and 13. (a) 13-*cis*-RA, (b) retinol, and (c) retinyl ester (RE). Data are for 130 embryos per group and are shown as mean ± SD, n=3 groups per timepoint and NF stages are indicated on the x-axis.

Figure S3: Cyp26c1 knockdown in Animal Caps Results in loss of Six1 and Pitx2c

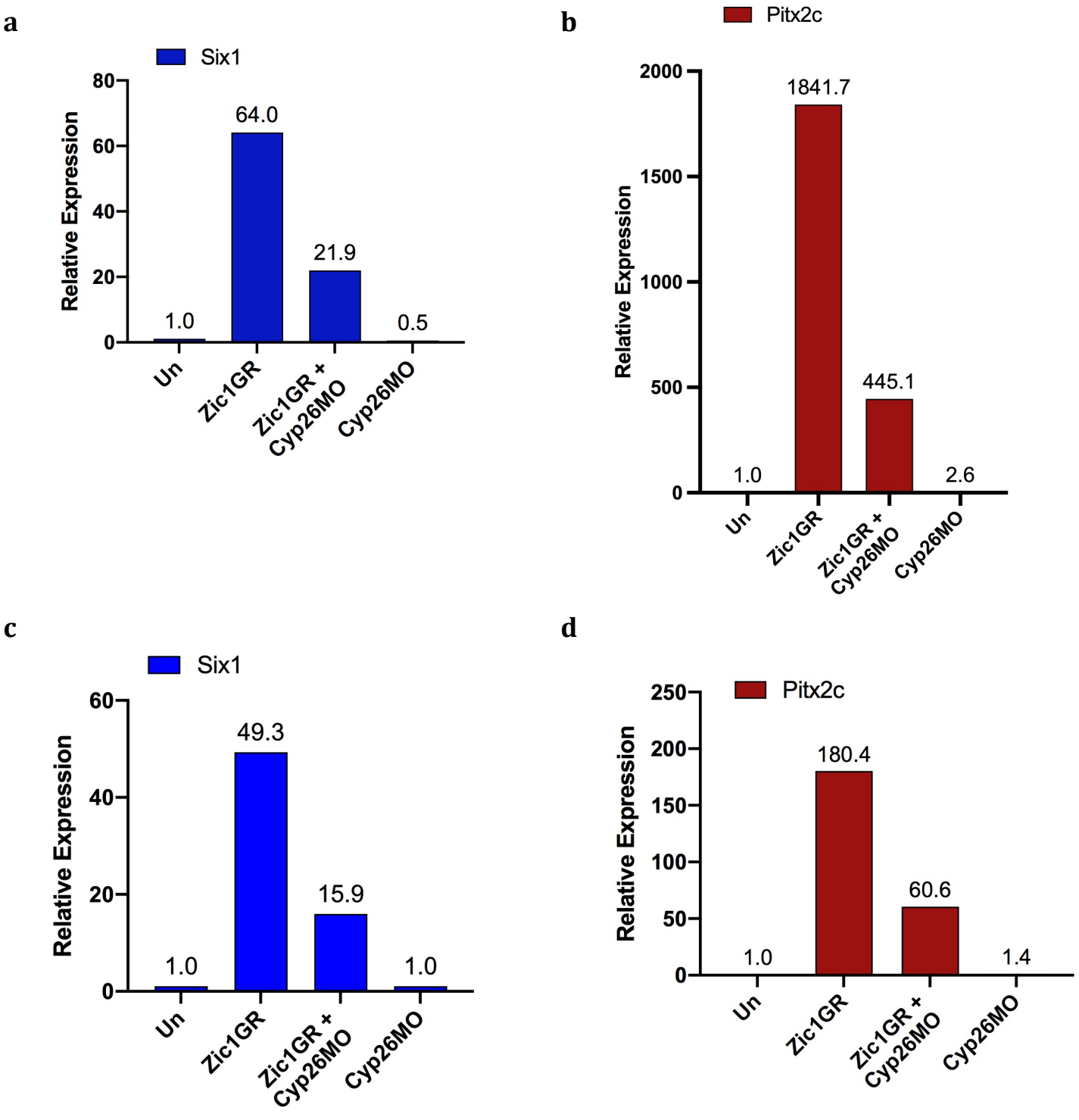

Figure S3: qRT-PCR analysis of *six1* (a, c) and *pitx2c* (b, d) expression in Zic1GR and Zic1GR+Cyp26MO injected animal caps from two biological replicates (a, b and c, d). Expression levels are normalized to ODC.

Figure S4: Cyp26c1 CRISPR/Cas9 Knockout validated by Direct Sequencing of PCR Product (DSP) Assay

Figure S4: Verification of sgRNA-mediated knockout of Cyp26c1 via DSP assay. Sanger sequencing of genomic DNA (gDNA) obtained from single embryos (1 to 3) injected with either Cas9 alone or with SL1 (a) or SL2 (b). For each sgRNA, the sequence of Cyp26c1 S form (Cyp26c1.S) was used as reference, annotated with the respective sgRNA target (gray bar) and PAM sequence (red bar). Sequencing traces of gDNA obtained from single embryos injected with both sgRNA (SL1, a; SL2, b) show occurrence of indels (insertion or deletion of bases) around the PAM site, which are absent in gDNA obtained from embryos injected with Cas9 only. The base and amino acid mismatches are indicated. Alignments were compiled using Geneious Prime.

Figure S5: Zic1 mediated induction of Six1 and Pitx2c is dependent on RA

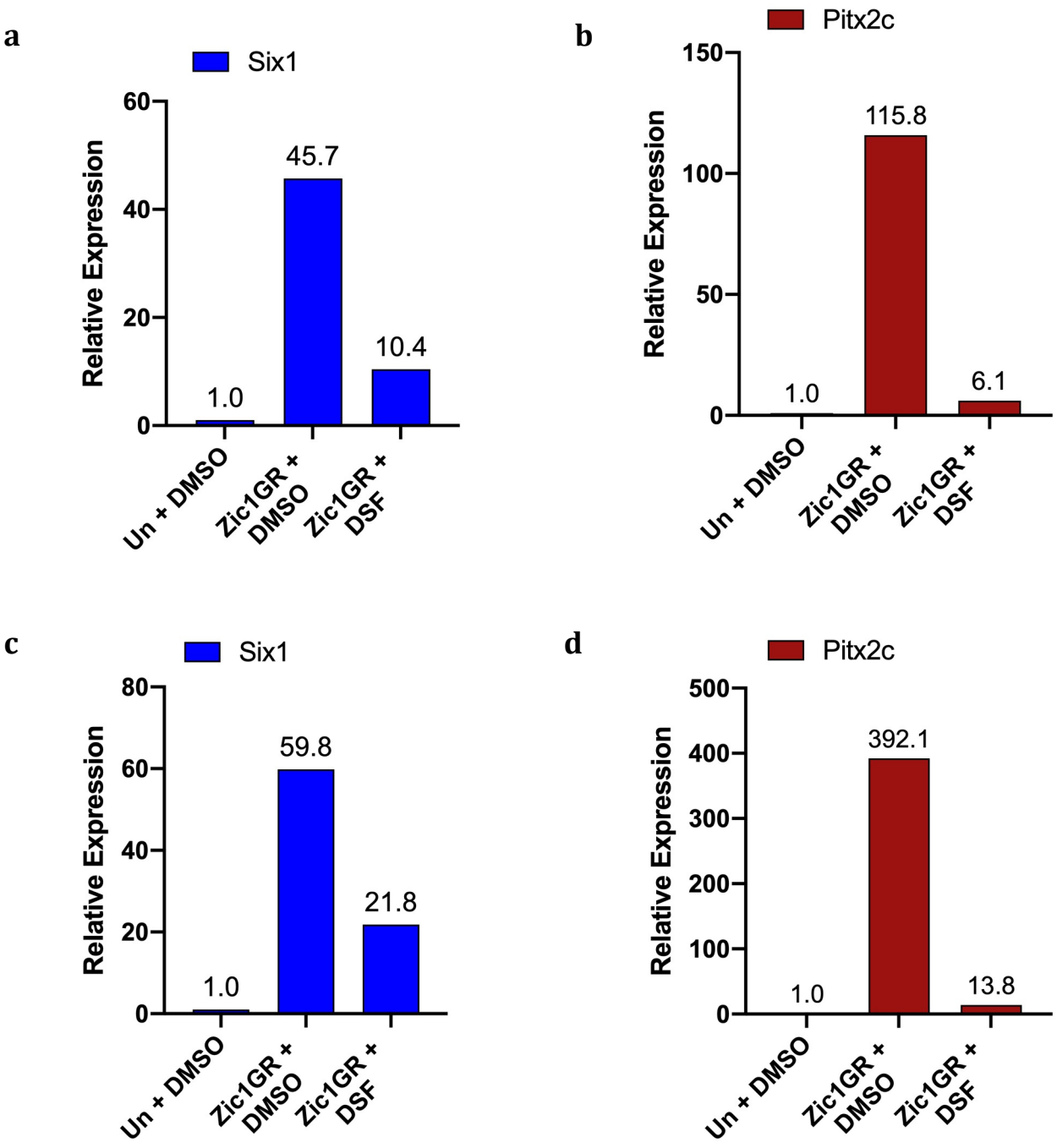

Figure S5: qRT-PCR analysis of *six1* (a, c) and *pitx2c* (b, d) expression) expression in animal cap explants injected with Zic1GR mRNA and cultured for 8 hours with or without Disulfiram (DSF; 100µM). Two biological replicates are shown (a, b and c, d), with values normalized to ODC.

Figure S6: Validation of Pitx2c splice-blocking morpholino

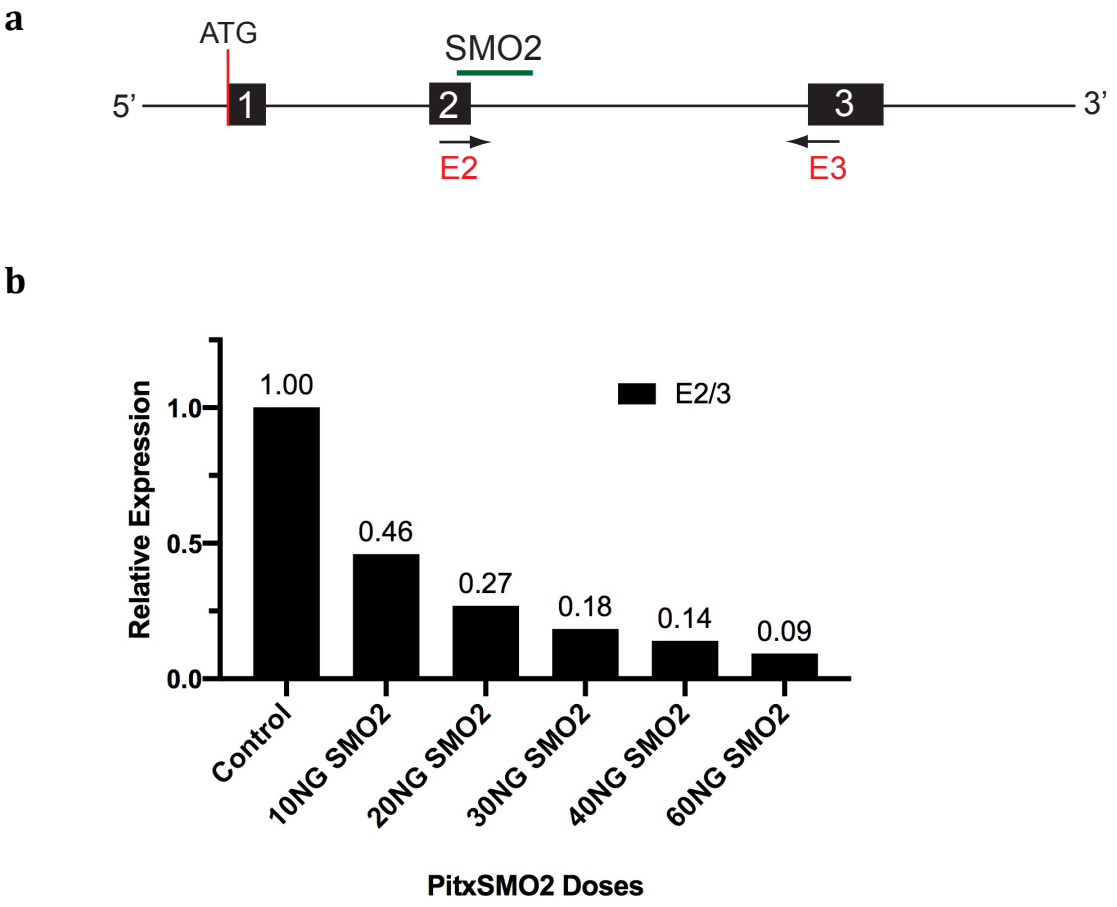

Figure S6: (a) Schematic representation of the *pitx2c* gene structure, indicating the target site for the splice-blocking (SMO2; green bar) morpholino. The primers used to detect exon skipping are indicated in red (E2, E3). (b) qRT-PCR analysis of total RNA from embryos bilaterally injected with increasing doses of PitxSMO2 as shown.

Figure S7: Pitx2c induces Cyp26c1 and Fgf8a

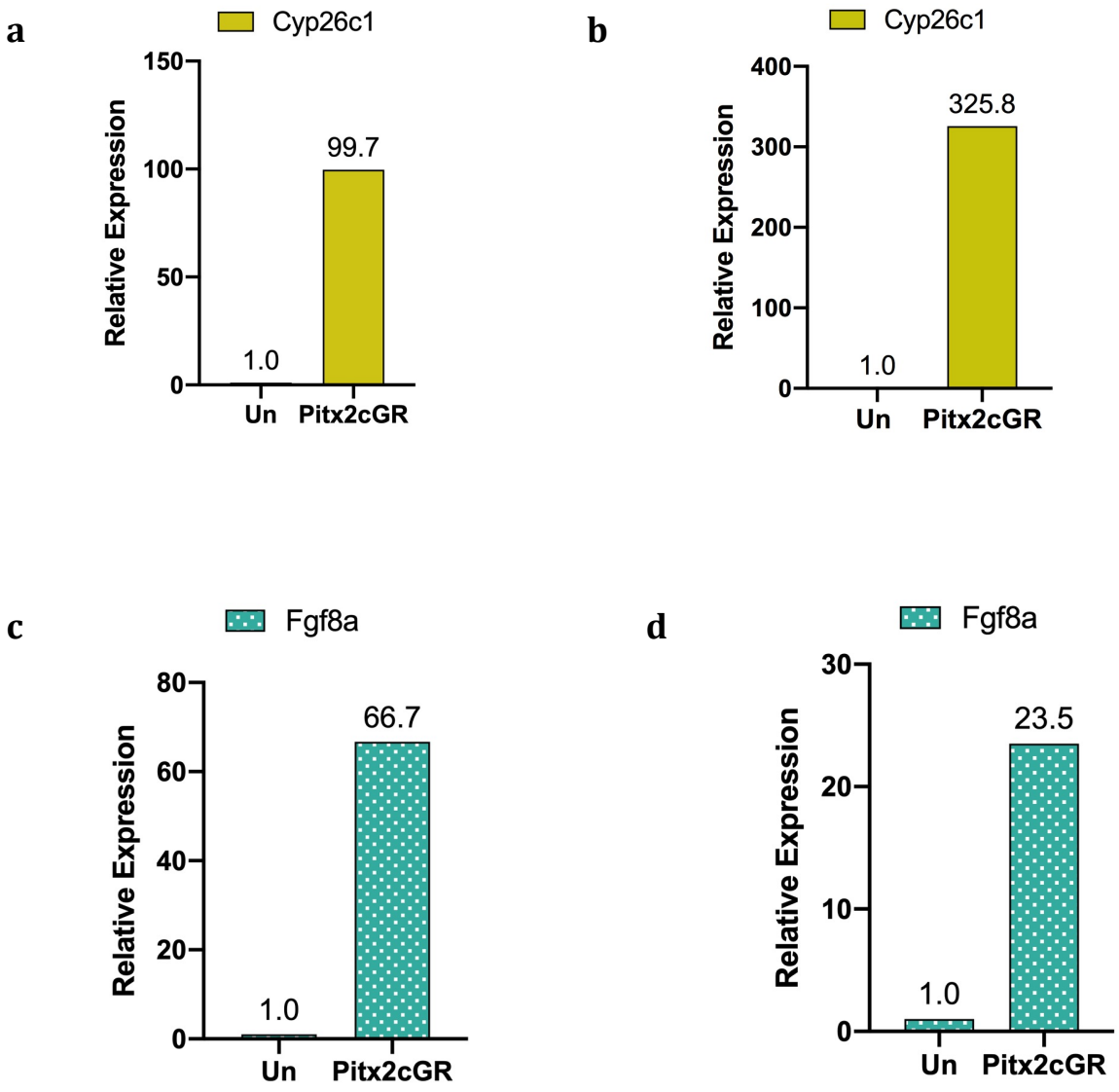

Figure S7: qRT-PCR analysis of *cyp26c1 and fgf8* expression in animal cap explants injected with Pitx2cGR mRNA and cultured for 8 hours and 4 hours, respectively. Two independent biological replicates are shown for cyp26c1 (a, and b) and fgf8 (c, and d). Values are normalized to ODC.

Figure S8: Pitx2c mis-expression in the whole embryo leads to cyp26c1 expansion and Fgf8 reduction

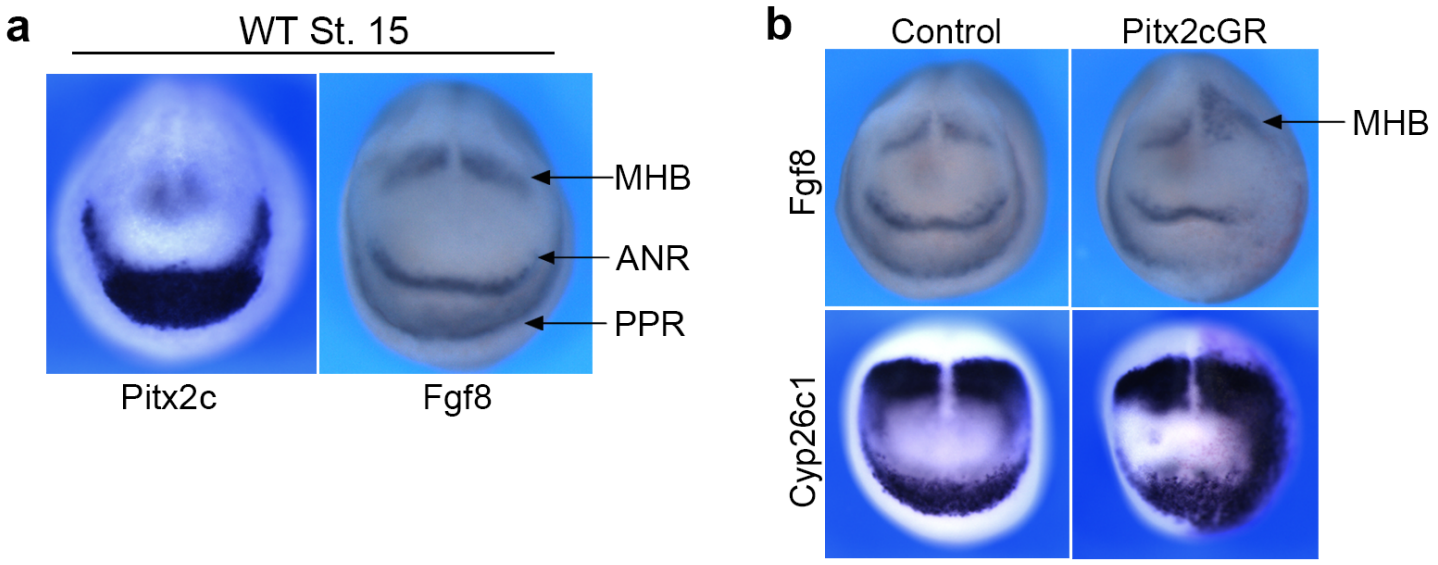

Figure S8: (a) Fgf8 is expressed in three nested domains: the prospective midbrain/hindbrain boundary (MHB), the anterior neural ridge (ANR) and the PPR (Ahrens and Schlosser, 2005), and the most anterior domains partially overlap with Pitx2c. (b) Pitx2c mis-expression in the whole embryo induces a posterior shift of Fgf8 MHB expression domain and a reduction of its ANR and PPR domains (upper panels), associated with a massive expansion of cyp26c1 expression domain (lower panels). Images show anterior views, dorsal to top.

Figure S9: SU5402 blocks the induction of Cyp26c1 by Pitx2c

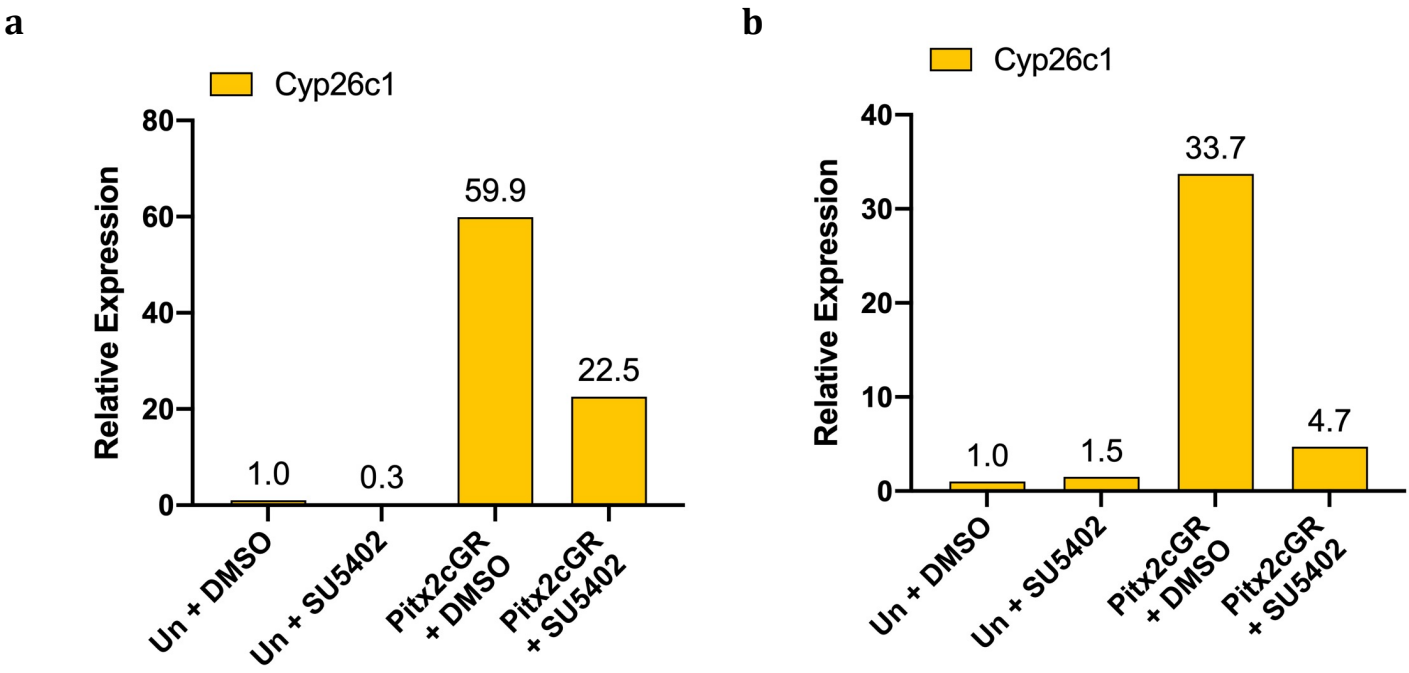

Figure S9: qRT-PCR analysis of *cyp26c1* expression in animal cap explants injected with Pitx2cGR mRNA and cultured for 8 hours with DMSO or SU5402 (25μM). Two independent experiments are shown (a, and b). Values are normalized to ODC.

Figure S10: Loss of Cyp26c1 does not affect the rate of cell death or proliferation in the ectoderm

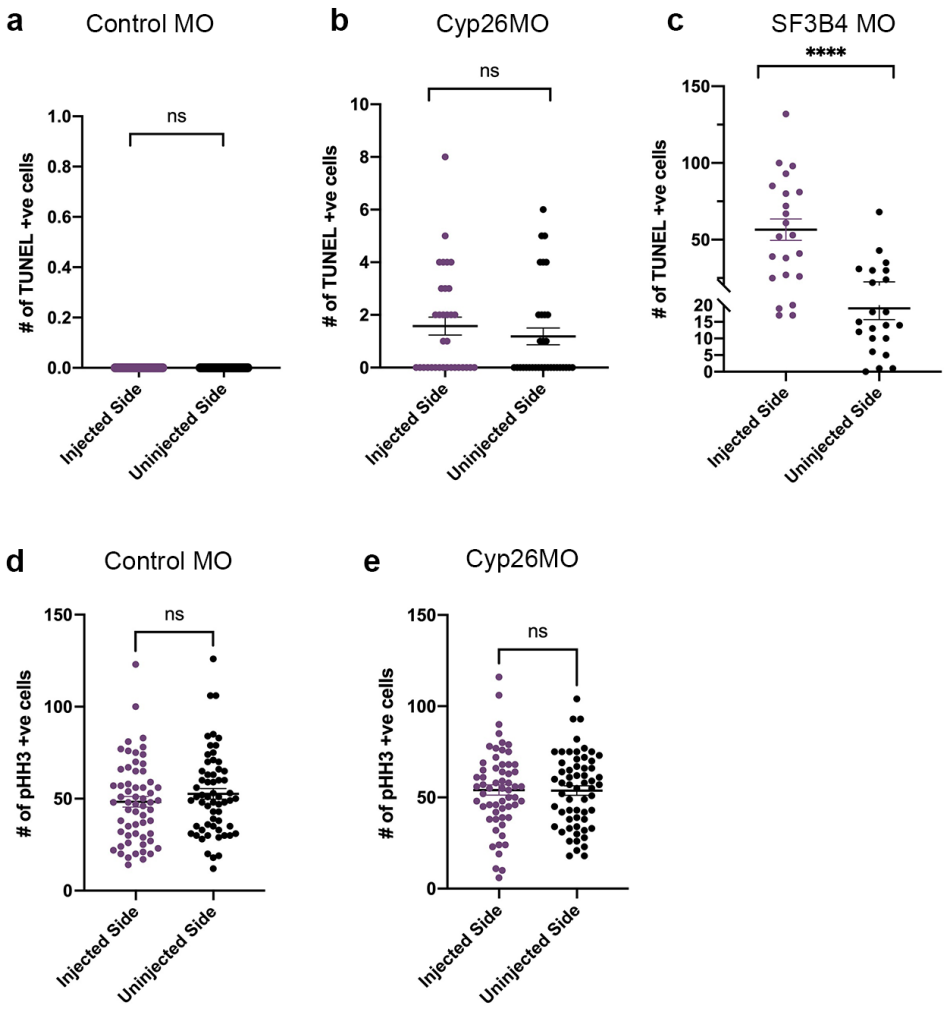

Figure S10: TUNEL (a-c) and pHH3 (d-e) staining of Cyp26c1-depleted *Xenopus* embryos. Embryos injected with CoMO (a) and Cyp26cMO (b) show no difference in the number of TUNEL-positive cells on injected vs. control sides. Injection of SF3B4MO (c) was used as a positive control (Devotta et al., 2016). A representative experiment of three biological replicates is shown. Similarly, embryos injected with CoMO (d) and Cyp26cMO (e) show no difference in the number of pHH3-positive cells on injected vs. control sides. Combined values from three biological replicates are shown. Each dot represents one embryo. p-values were calculated using unpaired t-test, **** $p<0.0001$, ns: not significant.

Figure S11: Cyp26c1 knockdown results in loss of *pitx2c* expression

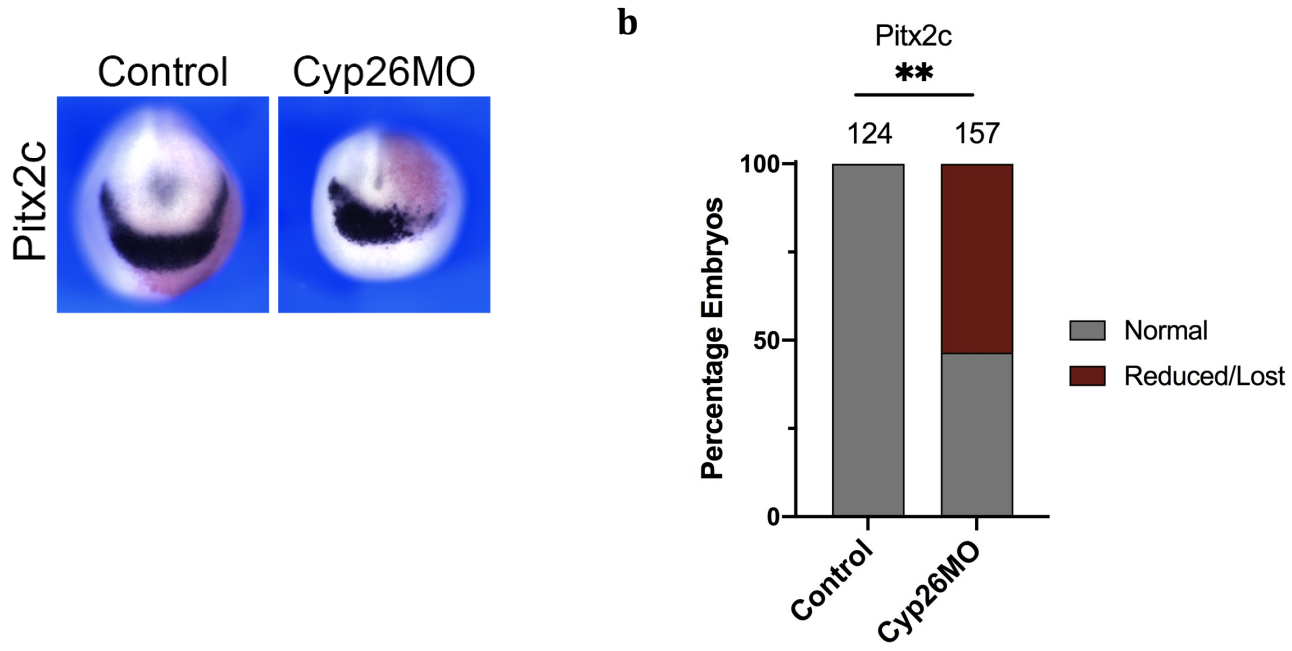

Figure S11: (a) ISH for *pitx2c* expression in control or Cyp26c1MO-injected embryos. The injected side is on the right showing Red-Gal. b) Quantification of the phenotypes for control versus Cyp26MO injected embryos. The total number of embryos (n) is indicated on the top of each bar. Data are from at least three biological replicates. p-values were calculated using unpaired t-test for major phenotype, ** p≤0.01. Images show anterior views with dorsal to top.

Table S1. Primers

Gene	Forward primer	Reverse primer
six1	5′ CTGGAGAGCCACCAGTTCTC 3′	5′ AGTGGTCTCCCCCTCAGTTT 3′
pitx2c	5′ ACTGTCCTCCCAGAGTATGT 3′	5′ GTTGCTGAGATTGTTCAGGTTATT 3′
cyp26c1	5′ ACAGTTCCAGGAGAGAGAAGTA 3′	5′ AGGCTGTGTTCTCCCAATAAG 3′
fgf8a	5′ GACTGCGTCTTCTCGGAAAT 3′	5′ CCCTTCTTGTGAAAGCCATAAAC 3′
ODC	5′ ACATGGCATTCTCCCTGAAG 3′	5′ TGGTCCCAAGGCTAAAGTTG 3′